

LEVEL II

12

ADA 058043

DESIGN CHARTS AND BOUNDARIES FOR IDENTIFYING
DEPARTURE RESISTANT FIGHTER CONFIGURATIONS

JULY 1978

By
William Bihrlle, Jr. and Billy Barnhart

Prepared under
Contract N62269-77-~~2276179~~ **C-0106**

DDC
RECEIVED
AUG 24 1978
RESOLVED

Prepared for
Naval Air Development Center
Department of the Navy
Warminster, Pennsylvania

Prepared by
Bihrlle Applied Research, Inc.
400 Jericho Turnpike
Jericho, New York

393371

**BEST
AVAILABLE COPY**

78 17 08 106

AD No.
DDC FILE COPY

ACKNOWLEDGEMENTS

The authors wish to acknowledge the cooperation of NADC personnel, especially A. Piranian, J. Clark and J. M. Stifel, who monitored this study during different periods of time. Also, gratefully acknowledged are the efforts of A. Sachleben of BAR in obtaining computer time histories and reducing same.

ACCESSION NO.	
NTIS	Write Section <input checked="" type="checkbox"/>
DOC	Duff Section <input type="checkbox"/>
UNANNOUNCED	<input type="checkbox"/>
JUSTIFICATION.....	
BY.....	
DISTRIBUTION/AVAILABILITY CODES	
Dist.	AVAIL. no./or SPECIAL
A	

MISSING PAGE BLANK-NOT FILMED

SUMMARY

A study is reported which generated design charts and developed associated boundaries for identifying departure and uncoordinated roll-reversal flight characteristics as a function of three aerodynamic parameters. This information should be valuable for specification, design and evaluation purposes.

The investigation utilized a large angle, six-degree-of-freedom digital computer program to simulate the motions of a fighter performing a severe air combat maneuver for different combinations of rolling and yawing coefficient and lateral control characteristics. It was demonstrated that a directionally stable airplane at high alpha is virtually immune to departure. For a directionally unstable configuration, a high dihedral effect will also prevent departures. The existence of proverse lateral control yaw characteristics minimizes the values of directional and lateral stability required to avoid departure or uncoordinated roll reversal.

TABLE OF CONTENTS

	<u>Page</u>
ACKNOWLEDGEMENTS	iii
SUMMARY	iv
LIST OF TABLES	vi
LIST OF FIGURES	vii
INTRODUCTION	1
SYMBOLS	2
TECHNICAL APPROACH	3
Introduction.	3
Aerodynamic Models	4
Inertia Parameter Models	7
Flight Condition and Maneuver	7
Parameter Investigation	8
Procedure for Developing Design Charts	9
Presentation of Results	9
DISCUSSION	11
Design Charts	11
Departure Boundary	13
Uncoordinated Roll Reversal Boundary	16
CONCLUSIONS	17
REFERENCES	19
APPENDIX A	A-1

LIST OF TABLES

<u>Table No.</u>		<u>Page</u>
I	Airplanes for Which Data Was Available	20
II	Mass Characteristics of Inertial Models	21
III	Matrix of Parameters Investigated	22

LIST OF FIGURES

Figure No.		Page
1	Inertia parameter models.	23
2	Design charts for determining departure susceptibility	24
3	Effect of the rate of onset in the loss of lateral stability on design chart information.	28
4	Constant alpha peak and damping ratio curves derived from design charts as a function of lateral and directional stability.	30
5	Departure boundaries.	32
6	Effect of inertia parameter models on design chart information.	34
7	Effect of maintaining directional stability to a higher alpha on design chart information.	36
8	Effect of maintaining directional stability to a higher alpha on departure boundary.	40
9	Uncoordinated roll reversal boundary.	41
A1	Rolling moment coefficient as a function of angle of attack for various airplanes. $\beta = 10$ deg.	A-3
A2	Yawing moment coefficient as a function of angle of attack for various airplanes. $\beta = 10$ deg.	A-4
A3	Rolling moment coefficient models for $\beta = 10$ deg.	A-5
A4	Rolling moment coefficient models for $\beta = 25$ deg.	A-6
A5	Yawing moment coefficient models for $\beta = 10$ deg.	A-7
A6	Yawing moment coefficient models for $\beta = 25$ deg.	A-8
A7	Yawing moment due to lateral control derivative models	A-9

LIST OF FIGURES (CONT.)

<u>Figure No.</u>		<u>Page</u>
A8	Normal force coefficient as a function of angle of attack and sideslip angle. $i_s = 0$ deg.	A-10
A9	Normal force coefficient as a function of angle of attack and sideslip angle. $i_s = -30$ deg.	A-11
A10	Axial force coefficient as a function of angle of attack and sideslip angle. $i_s = 0$ deg.	A-12
A11	Axial force coefficient as a function of angle of attack and sideslip angle. $i_s = -30$ deg.	A-13
A12	Pitching moment coefficient as a function of angle of attack and sideslip angle. $i_s = 0$ deg.	A-14
A13	Pitching moment coefficient as a function of angle of attack and sideslip angle. $i_s = -30$ deg.	A-15
A14	Side force coefficient as a function of angle of attack and sideslip angle. $i_s = 0$ deg.	A-16
A15	Side force coefficient as a function of angle of attack and sideslip angle. $i_s = -30$ deg.	A-17
A16	Rolling moment due to lateral control derivative as a function of angle of attack and control deflection. $i_s = 0$ deg.	A-18
A17	Rolling moment due to lateral control derivative as a function of angle of attack and control deflection. $i_s = -30$ deg.	A-19
A18	Side force due to lateral control derivative as a function of angle of attack and control deflection. $i_s = 0$ deg.	A-20
A19	Side force due to lateral control derivative as a function of angle of attack and control deflection. $i_s = -30$ deg.	A-21
A20	Damping derivative, C_{m_q} , as a function of angle of attack.	A-22

LIST OF FIGURES (CONT.)

<u>Figure No.</u>		<u>Page</u>
A21	Damping derivative, $C_{\dot{\alpha}_p}$, as a function of angle of attack.	A-23
A22	Cross derivative, C_{n_p} , as a function of angle of attack.	A-24
A23	Cross derivative, $C_{\dot{\alpha}_r}$, as a function of angle of attack.	A-25
A24	Damping derivative, C_{n_r} , as a function of angle of attack.	A-26

INTRODUCTION

High angle-of-attack capability has been shown to significantly enhance the air combat maneuvering (ACM) effectiveness of fighter airplanes (e.g. see ref. 1). Unfortunately, it has not been possible to design for such a capability with any degree of confidence. This is primarily attributable to the fact that there is no criterion which identifies the susceptibility of a specific design to depart from controlled flight when performing rolling maneuvers. Consequently, departures are first discovered during flight tests of the full-scale article. At this point in the airplane development cycle, the only recourse is to incorporate a device which alerts the pilot to an approaching dangerous flight regime, or to automatically limit the control authorities. Nevertheless, under certain conditions, pilots do inadvertently enter the flight regime where departures and, consequently, spins occur. Also, an alpha limitation imposed by departure susceptibility denies full use of a configuration's inherent ACM capability.

It should be recognized that any airplane will begin to rotate (i.e. change heading) at high alpha and enter a large angle motion if a yawing moment can be generated and held sufficiently long through the application of asymmetric power or displacement of an effective aerodynamic control. The motion of concern, however, is one in which the existence or direction of a yawing motion is contrary to what had been anticipated, and the motion occurs so quickly that the airplane is in an incipient spin phase before the pilot can take corrective action. The objectives of the efforts reported herein, therefore, are to develop design charts and associated departure boundaries with which to identify a particular design's degree of susceptibility to this departure phenomenon. Such data would be useful as an evaluation, specification and design tool.

SYMBOLS

b	wing span	ft
m	mass	slugs
q	free-stream dynamic pressure	lb/ft ²
S	wing area	ft ²
\bar{c}	wing mean aerodynamic chord	ft
C_l	rolling moment coefficient, rolling moment (qSb)	
C_n	yawing moment coefficient, yawing moment/(qSb)	
$C_{l\beta}$	lateral stability derivative, $\partial C_l / \partial \beta$	per deg
$C_{n\beta}$	directional stability derivative, $\partial C_n / \partial \beta$	per deg
$C_{n\delta_a}$	yaw due to lateral control derivative, $\partial C_n / \partial \delta_a$	per deg
I_X, I_Y, I_Z	moment of inertia about X, Y, and Z body axis, respectively	slug-ft ²
I_{XZ}	product of inertia, positive when the principal X axis is inclined below the X body axis at the aircraft nose	slug-ft ²
R_E	Reynolds number	
α	angle of attack, positive when X body axis is above projected relative wind vector	deg
β	sideslip angle, positive when the relative wind vector is to the right of the X-Z plane.	deg
δ_a	lateral control deflection, positive to produce left (negative) rolling moment	deg

TECHNICAL APPROACH

Introduction

- The technical approach used for this study consisted of:
- o selecting key aerodynamic models,
 - o analytically generating airplane time responses for combinations of these models while performing a severe ACM,
 - o tabulating and analyzing the responses,
 - o constructing departure susceptibility design charts, and
 - o developing departure boundaries from these charts.

The departure susceptibility design charts were based on the results of large angle, six-degree-of-freedom computations, since departure from controlled flight and attendant incipient spin motions are large amplitude, coupled motions which reflect the influence of gyroscopic and kinematic effects. Airplane departures are not, for example, the result of a gust disturbance which develops into a large amplitude motion through the means of an unstable oscillation. The employment of linearized, limited degree-of-freedom equations of motion, consequently, would not identify the departure phenomenon.

It was believed that most of the important aerodynamic parameters involved in the departure phenomenon had already been identified. For instance, a large angle, six-degree-of-freedom analytical study (ref. 2) sponsored by NASC in 1967 determined that adverse yaw due to lateral control, dihedral effect and directional stability were the critical aerodynamic characteristics involved in promoting a spin. Analytical and flight test investigations since then have corroborated these findings.

It was assumed that control induced departures are functions of the relative magnitude of these key aerodynamic param-

eters and their variation with angle of attack, as well as the airframe's inertial characteristics. Consequently, this study endeavored to determine how the relative values of these aerodynamic and inertial variables influence departure susceptibility. The ability to construct departure susceptibility design charts was predicated on ascertaining that a reasonable number of aerodynamic (C_ℓ , C_n and $C_{n\delta_a}$) and inertial models could represent the spectrum of fighter-type airplanes.

Aerodynamic Models

The aerodynamic models discussed in this section are presented in Appendix A. All of the aerodynamic parameters were a function of angle of attack and, depending upon the parameter, such other variables as control deflection and/or sideslip angle. Since supersonic flight was not investigated, Mach number effects were not included in the models.

The first phase of the study was the selection of the C_ℓ , C_n and $C_{n\delta_a}$ models to be investigated. Models were desired which would encompass all possible fighter configurations. To accomplish this, high angle-of-attack data for fighter-type airplanes were sought. The airplanes for which data were obtained are listed in Table I; some of these data are presented in plotted form in Appendix A. High R_E data were desired so as to insure that the models chosen represented full-scale airplane characteristics. The models were constructed on the basis of these data. Since all of the data fell into a broad band throughout the angle-of-attack range, it was possible to represent the aerodynamic characteristics of all the airplanes with a reasonable number of models. As shown in Table I, low R_E data was also obtained. It is interesting to note that this data fell within the selected models for angles of attack of 40 deg

and above.

Rolling Moment Coefficient

The rolling moment coefficient, C_{ℓ} , was modelled as a function of α and β . The general trend, for a given level of positive sideslip, was for C_{ℓ} to be negative (stable) at an angle of attack of zero degrees and become increasingly so with increasing alpha up to approximately the stall region, after which no further increase in stability was realized; or, more generally, a decrease in stability was experienced for increasing alphas. In no case was C_{ℓ} found to become positive (unstable).

The models chosen for the rolling moment coefficient all began at the same value at zero angle of attack and reached their maximum stable value at the same alpha, with one exception. The exception was Model A, which represented a slatted configuration. For this case, C_{ℓ} , continued to increase in a stable sense past the stall alpha of the unslatted configuration, reaching its maximum at a higher angle of attack, then returning to the level of the unslatted C_{ℓ} at even higher alphas. The models selected encompassed all of the airplane rolling coefficient characteristics and, in some instances, closely approximated actual configurations (e.g. F-14, F-15, F-111).

Yawing Moment Coefficient

The yawing moment coefficient, C_n , is modelled as a function of angle of attack and sideslip. As one would expect, for a given positive sideslip angle, the airplane data shows C_n to be positive (stable) at low alphas until approximately the stall; stability then decreases generally to an unstable value at high alphas. This loss of directional stability probably can be traced to adverse sidewash due to a vortex impinging on the

vertical tail surface after wing panel stall. The level of instability reached and the angle of attack at which the loss of stability begins vary from configuration to configuration. The YA-10 configuration deviates from the norm in that it exhibits directional stability throughout the alpha range.

The yawing moment models were chosen to cover the band of data, from a constant, stable C_n for all alphas, to a neutrally stable case (C_n equal to zero), to the more common situation which starts stable, then becomes unstable in the post-stall alpha range. (For this latter situation, only one level of stability below 20 degrees angle of attack was investigated since the ACM maneuver employed herein exceeded this alpha range before a sideslip value was generated.) Several different combinations of the level of instability and the angle of attack at which loss of stability begins were modelled.

Yaw Due to Lateral Control

Yaw due to lateral control, $C_{n\delta_a}$, values were chosen to represent typical characteristics exhibited by fighter airplanes. Three models were chosen: neutral, ($C_{n\delta_a}$ identically zero); proverse ($C_{n\delta_a}$ remains negative throughout the alpha range); and adverse ($C_{n\delta_a}$ initially negative and becoming highly positive in the post-stall alpha range).

Aerodynamics Not Varied

The lift, drag and longitudinal control power characteristics, as well as the dynamic derivatives, were typical of those associated with many current fighter airplanes and were not varied during this study. The airplane was statically stable in pitch throughout the angle-of-attack range and not control limited so that the airplane could be trimmed to approximately 40 degrees angle of attack. It should be noted that $C_{l\delta_a}$ was also

not varied although different levels of $C_{n\delta_a}$ were investigated.

Inertia Parameter Models

The distribution of mass along the body reference axes for various airplane configurations and the models chosen are presented in figure 1. As shown, mass is always distributed along the fuselage axis for fighters, but to varying degrees. This distribution can be covered with three inertia parameter models. Model A represents a configuration which has its mass distributed only slightly more in the fuselage than in the wings. Model C represents a configuration whose mass is concentrated heavily in the fuselage. Since the Model B configuration lies between the two extremes, it was used extensively in the aerodynamic parameter study. The mass characteristics for this model are presented in Table II.

In order to determine the influence of mass distribution on an ACM, the multiplicative factors presented in Table II were used to simulate Models A and C. These factors multiplied only the contribution of the inertia coupling (gyroscopic) terms in the equations of motion. In this manner, the gyroscopic effect of Model B could be magnified or diminished without having to change the inertia values, I_x , I_y or I_z , which would have simultaneously incurred unrealistic corresponding changes in the aerodynamic acceleration and damping characteristics.

Flight Condition and Maneuver

The airplane was trimmed in a 60-degree bank angle turn at 35,000 feet and Mach 0.9 before a rolling pull-out type maneuver was performed. Control inputs for this maneuver were:

- o Full trailing-edge-up longitudinal control deflection initiated at time equal zero at a rate of 30 deg/sec.
- o Full lateral control deflection initiated at time equal 1.5 sec at a rate of 30 deg/sec in the direction to unbank the airplane.
- o Rudder remained undeflected.

The controls remained fully deflected until eight seconds into the time history, at which time both the longitudinal and lateral controls were returned to trim at 30 deg/sec.

This maneuver was chosen because it represented an ACM from which departures are often experienced. It is also severe: controls are fully deflected, the airplane is pitched up rapidly through the stall and, being uncoordinated, large sideslip angles are generated.

Parameter Investigation

A matrix of the aerodynamic and inertia parameter model variations investigated is shown in Table III. To evaluate these parameter variations, 20-second time histories of the airframe motions were generated in response to the previously described control inputs. These motions were computed using a large angle, six-degree-of-freedom digital computer program at the NADC computer facility. The program used non-linear tabulated data for the aerodynamic, atmospheric and control inputs. When required, aerodynamic parameter tables could be programmed as functions of up to three independent variables (e.g., angle of attack, angle of sideslip and control deflection). Control deflection input tables were programmed as a function of time.

The resultant time history output (i.e. the vehicle response to the control inputs) were plotted on a CALCOMP drum plotter. Up to 64 output parameters of interest could be plotted against time for each computer run. For the purpose of this study, the following sixteen parameters were plotted because they were deemed to be of particular significance:

pitch angle	elevator deflection
bank angle	lateral control deflection
yaw angle	flight path angle
pitch rate	altitude change
roll rate	range position
yaw rate	dynamic pressure
angle of attack	velocity
sideslip angle	rotation rate

Procedure for Developing Design Charts

Each parameter's influence on the computed time history was determined by examining the path of the center of gravity and the airplane's motions about the center of gravity, using the traces cited in the previous section. The following time history parameters, considered to be significant indicators of these motions, were then tabulated:

- peak yaw rate magnitude and sign
- time to maximum yaw rate
- time at which yaw rate exceeded +1 rad/sec
- last alpha peak value prior to lateral control removal
- approximate second order damping ratio of alpha trace
- time for bank angle to reach zero deg (and whether reversal occurred)
- incremental peak bank angle attained before lateral control was removed

These parameters, in turn, were then reviewed to determine if the airplane had departed from controlled flight. Subjectively, the concept of airplane departure is easily defined; it means the pilot has lost positive control of the airplane. Although an objective definition of departure was not available, four of the above seven time-history parameters (identified by ●) were found to be the most useful in identifying departure susceptibility. These parameters were plotted for each model investigated and were used as departure susceptibility design charts. These charts were used to construct departure boundaries.

Presentation of Results

Figure 2 presents departure susceptibility design charts in terms of the following time-history parameters:

Figure 2a - last alpha peak prior to lateral control re-

moval

Figure 2b - approximate second order damping ratio of alpha trace

Figure 2c - peak yaw rate

Figure 2d - incremental peak bank angle reached at time lateral control removed

These figures present the value of the time history parameter of interest for the combinations of aerodynamic models (C_n , C_l , $C_{n\delta_a}$) shown by the matrix of computer runs in Table III for inertia parameter Model B, excluding unstable C_n models (2) and (3). Each of the figures contains three plots: one each for the unstable, neutral and stable C_n models investigated. Each of these plots, in turn, presents the value of the time-history parameter for each combination of $C_{n\delta_a}$ and C_l models studied by presenting the time-history parameters as a function of the C_l model for constant values of $C_{n\delta_a}$. To facilitate interpretation, the C_l models are spaced along the abscissa according to the value of the $C_{l\beta}$ slope of the C_l models at 40 degrees angle of attack, with each model indicated by symbols according to the key. The 40 degree alpha $C_{l\beta}$ value was chosen because: (1) the models exhibit constant $C_{l\beta}$ vs α characteristics for a given level of sideslip above this angle of attack and (2) because the angle of attack is either converging to a trim level of approximately 40 degrees or diverging to a higher alpha at the time the controls are returned to trim.

DISCUSSION

Design Charts

Figures 2a and 2b show how the angle-of-attack behavior varies for different combinations of the aerodynamic models. For a stable C_n model, the angle-of-attack time history traces are damped and the angle of attack approaches its trim value of approximately 40 degrees regardless of the C_ℓ and $C_{n\delta_a}$ models employed. For neutral or unstable yawing moment models, C_ℓ becomes the most important parameter in determining if the alpha time history is convergent or divergent. If C_n is unstable above the stall, as is the case for most airplanes, a fairly high level of dihedral effect is required to prevent the airplane from diverging in angle of attack to levels where spins could occur. The $C_{n\delta_a}$ level also influences the degree of divergence and the magnitude of the peak alpha value, but to a lesser extent than the C_ℓ level.

Figures 2c and 2d show that the direction in which the airplane rolls and yaws in response to the control inputs also depends strongly upon the C_n characteristics. For a stable yawing moment model, the airplane will roll in the direction commanded (negative) accompanied by a coordinating (negative) yaw rate, whereas the opposite occurs for an unstable yawing moment model. These responses (both the favorable and the undesirable) are significantly minimized with increasing dihedral effect. As $C_{n\delta_a}$ becomes less proverse, a favorable response is also minimized; but, in this case, an undesirable response is maximized. For the neutral C_n model, the peak bank angle and yaw rate, in general, do not vary much

with the $C_{l\beta}$ level (for $C_{l\beta}$ greater than $-.0015$), but are significantly influenced by the $C_{n\delta_a}$ model. The airplane rolls in the direction commanded and experiences a coordinating yaw rate for the proverse $C_{n\delta_a}$, whereas the opposite occurs for adverse $C_{n\delta_a}$. For $C_{n\delta_a}$ equal to zero, the overall response in roll and yaw averaged out to approximately zero by the time the lateral control was neutralized.

These design charts show that a stable yawing moment characteristic is the most effective parameter governing departure prevention. It also tends to prevent control reversal during an uncoordinated rolling maneuver at high alphas. A designer's recourse when confronted with a configuration directionally unstable over some alpha range is to insure a high level of dihedral effect. For this combination of aerodynamic characteristics, departures are eliminated at the expense of inducing roll reversal. This constitutes a trade-off between a safety-of-flight condition and a flight characteristic that might be regarded as annoying (i.e. use of rudder pedals required). It is evident that these design charts can be used for configuration studies in which directional stability, dihedral effect and lateral control characteristics may be traded-off for the high alpha maneuvering responses desired.

The design charts in figure 2 present only the C_l models which differed at high angle of attack (≥ 40 degrees). The influence of the rate of onset of these high alpha C_l values are not shown. This situation was investigated for the unstable C_n and adverse $C_{n\delta_a}$ models. Figure 3 presents the same four time-history parameters as those presented in figure 2, plotted against the angle of attack at which the C_l model assumed its high alpha value for a given sideslip angle. As can be seen, the low alpha portion of the C_l curve does in-

fluence the magnitude of the angle-of-attack characteristics, bank angle and yaw rate, but it does not change the results: angle of attack still diverges for all cases and the airplane experiences a roll reversal for this uncoordinated maneuver. A departure boundary based solely on figure 2 data would, therefore, still be valid despite exclusion of this C_{ℓ} model characteristic.

Departure Boundary

Yaw rate alone is not a good indicator of departure, since many combinations of the aerodynamic parameters investigated result in yaw rates that are opposite (unfavorable) to the commanded lateral control displacement, but are accompanied by a roll reversal. Consequently, the airplane yaws in the same direction it rolls, and contrary to command. This roll reversal is not a departure; it is actually the "safety valve" that precludes departure and presents a strong signal to the pilot to enter the control loop and coordinate the maneuver.

Departures leading to incipient spins have a common characteristic: the angle of attack must be sustained above the high alpha trim point. Hence, the alpha time-history parameters were used to determine if departure had occurred. The model used for the study trimmed at an alpha of approximately 40 degrees. Departure was assumed if the alpha time history demonstrated progressively higher peak alphas from trim.

The angle-of-attack information contained in figures 2a and 2b were cross-plotted as functions of $C_{n_{\beta}}$ and $C_{\ell_{\beta}}$ for each $C_{n_{\delta_a}}$ model. $C_{n_{\beta}}$ was the slope of the C_n models at 40 degrees

alpha and was used for the same reasons previously discussed relative to $C_{l\beta}$. Values of $C_{n\beta}$ and $C_{l\beta}$ which resulted in attaining given levels of peak alphas were obtained from these cross plots and were plotted as boundaries, as illustrated in figure 4 for the adverse $C_{n\delta_a}$ model. Figure 4 also shows the $C_{n\beta}$ and $C_{l\beta}$ combinations which resulted in constant alpha trace damping ratios. In order to choose a departure boundary which considered both a divergent oscillation (i.e., negative damping) situation and an alpha build-up to high values, although oscillations were damped, it was decided to use the 50 degree alpha peak (10 degrees above trim) curves in conjunction with the zero damping ratio curves, choosing the most conservative as the departure boundary.

It should be noted that the aerodynamic model employed for this study consisted of static aerodynamics and dynamic derivatives. For this reason, conclusions concerning whether or not a spin occurs should not be drawn from these departure boundaries. To predict spins, it is necessary to model rotary aerodynamics, as has been shown in ref. 3.

A departure boundary for each level of $C_{n\delta_a}$ is shown in figure 5. For combinations of $C_{n\beta}$ and $C_{l\beta}$ above the boundary, departure does not occur. For combinations below the boundary, departure occurs for the maneuver used in this study. For less severe maneuvers, departure may not occur even for $C_{n\beta}$ and $C_{l\beta}$ combinations below the boundary, but the danger of departure would be present. As an example, several computer simulations were made for which the controls were removed at times

less than eight seconds (e.g. two and four seconds). For very short control input durations, departure would not occur for any combination of aerodynamic models investigated, since the airplane was unable to develop any sizable motions. However, as the input duration increased, departures would be experienced for the aerodynamic parameter combinations indicated by the boundaries.

The departure boundaries show that for large stable values of $C_{l\beta}$, fairly large unstable $C_{n\beta}$ values can be tolerated without departure susceptibility, regardless of $C_{n\delta a}$ characteristics. For low levels of $C_{l\beta}$, more stable (or at least less unstable) $C_{n\beta}$ values would be required for a configuration to remain departure resistant. For an airplane which exhibits a positive (stable) $C_{n\beta}$, the influence of $C_{l\beta}$ becomes unimportant except for a configuration with virtually no dihedral effect.

The results presented in figures 2 through 5 were derived using the inertia-parameter Model B. A limited number of time histories were generated for the inertia-parameter Models A and C. In figure 6, the angle-of-attack design chart parameters obtained for inertia-parameter Model B are compared with the values obtained with Models A and C. These data are presented since they were employed to develop the departure boundaries. As shown, significant differences were obtained only for Model C at some $C_{l\beta}$ values. Even these differences, however, would not significantly affect the departure boundaries which were based on zero damping or a 50 degree alpha peak value. Admittedly, the inertia-parameter model study was limited and further study would be warranted to fully document the importance of mass distribution on the departure boundaries.

The effect of maintaining directional stability to a higher alpha, unstable $C_{n\beta}$ model (2), is shown in figure 7. The design chart parameters show that maintaining directional stability to a higher angle of attack results in lowered peak alphas and an increased damping ratio, with an increased peak yaw rate and bank angle. As shown in figure 8, a sizable shift in the alpha at which directional stability is lost does not change the slope of the boundary and results in only a small shift.

Uncoordinated Roll Reversal Boundary

Examination of the design charts (figure 2) showed that for a large group of the cases studied the airplane rolled in a direction opposite to that commanded. The initial motion was in the commanded direction, to varying degrees; it then reversed and rolled in the opposite direction. This maneuver is uncoordinated and, therefore, large sideslip angles are generated at large alpha. A commanded negative roll rate at positive angles of attack produces a sideslip angle which, for an unstable $C_{n\beta}$, will introduce a positive yaw rate. This, in turn, leads to more negative sideslip and a positive rolling moment, due to dihedral effect (negative $C_{l\beta}$). An adverse $C_{n\delta_a}$ aggravates the situation by producing additional positive yaw rate due to the deflection of the lateral control. For a stable $C_{n\beta}$, this effect is combatted since the magnitude of the negative sideslip is depressed or positive sideslips are realized.

It is possible to generate boundaries using the bank angle information in figure 2 in the same manner as was done for the departure boundaries. These are shown in figure 9. It is emphasized that these boundaries are not departure boundaries but are uncoordinated roll-reversal boundaries requiring the pilot to apply rudder to coordinate the maneuver or to depress the angle of attack.

CONCLUSIONS

Departure susceptibility and uncoordinated roll-reversal boundaries have been developed from design charts generated by considering a series of roll and yaw coefficient characteristics for different types of yaw due to lateral control deflection. For ease of use, these boundaries are presented in terms of derivatives, i.e. $C_{\ell\beta}$, $C_{n\beta}$, $C_{n\delta_a}$. The boundaries and design charts can serve as valuable evaluation, specification and design tools. They were used to provide the following conclusions:

- o positive directional stability at high alpha prevents the airplane performing a severe ACM from diverging to alphas above trim and into the region where spins are encountered, regardless of the level of dihedral effect and the value of $C_{n\delta_a}$.
- o For directionally unstable configurations, a large dihedral effect (negative $C_{\ell\beta}$) can avert departure. However, this may require rolls to be coordinated to avoid roll reversal.
- o The presence of a proverse $C_{n\delta_a}$ characteristic minimizes the value of $C_{n\beta}$ and $C_{\ell\beta}$ required to avoid departure or uncoordinated roll-reversal.

As in all studies, the scope of the effort was influenced by the time and resources available. The limitations placed on the present study, however, did not compromise the applicability of the results and the development of boundaries and definitive conclusions. Nevertheless, the following limitations should be noted. Variations of the mass-inertial parameters within the range that characterize fighter airplanes seemingly do not change the boundaries which were determined.

Further study is required to make this conclusion unequivocally. The aerodynamic parameters C_{m_q} and C_{m_β} , while not treated herein, may cause displacement of the boundaries. Also, the boundaries were developed for airplanes that are stable in pitch throughout the angle-of-attack range (between 0 and 90 degrees) and have no limitation placed on the available longitudinal control authority. Pronounced changes in these characteristics would patently shift these boundaries.

REFERENCES

1. Bihrlle, William, Jr.: and Meyer, Rudolph C.: F-14A High-Angle-of-Attack Characteristics. Journal of Aircraft, Vol. 13, No. 8, Aug. 1976.

2. Bihrlle, William, Jr.: Influence of the Static and Dynamic Aerodynamic Characteristics on the Spinning Motion of Aircraft. Journal of Aircraft, Vol. 8, No. 10, Oct. 1971.

3. Bihrlle, William, Jr.; and Barnhart, Billy: Effects of Several Factors on Theoretical Predictions of Airplane Spin Characteristics. NASA CR 132521, Aug. 1974.

TABLE I.- AIRPLANES FOR WHICH DATA WAS AVAILABLE

High R_E data - 13 configurations

F-4E (slatted and unslatted)	F-5E
F-14 (slatted and unslatted)	YA-10
F-15 (Republic proposal)	TA-4
F-15	F-18
F-111	T-2C
F-5A	

Low R_E data - 15 configurations

F-92	A-7
F-102	F-4
F-4D	F-111
F-8	F-5
D-558	B-1
MIG	B-58
BELL D-188	F-100
X-15	

TABLE II.- MASS CHARACTERISTICS OF INERTIAL MODELS

INERTIAL MODEL B

$$I_X = 25,000 \quad (I_X - I_Y) / mb^2 = -0.067$$

$$I_Y = 135,000 \quad (I_Y - I_Z) / mb^2 = -0.012$$

$$I_Z = 155,000 \quad (I_Z - I_X) / mb^2 = 0.079$$

$$I_{XZ} = 0$$

$$m = 1025$$

INERTIAL MODEL A

$$(I_X - I_Y)_A = 0.407 (I_X - I_Y)_B$$

$$(I_Y - I_Z)_A = 1.0 (I_Y - I_Z)_B$$

$$(I_Z - I_X)_A = 0.438 (I_Z - I_X)_B$$

INERTIAL MODEL C

$$(I_X - I_Y)_C = 2.754 (I_X - I_Y)_B$$

$$(I_Y - I_Z)_C = 1.0 (I_Y - I_Z)_B$$

$$(I_Z - I_X)_C = 2.435 (I_Z - I_X)_B$$

TABLE III.- MATRIX OF PARAMETERS INVESTIGATED

$C_{n\delta_a}$ Model C_n Model		C_l Model for Inertia Parameter Model				
		B			A	C
		Adverse	Neutral	Proverse	Adverse	Adverse
Stable		A B C E E' E''	A B C E E' E''	A B C E E' E''		
Neutral		A B C D E E' E''	A B C E E' E''	A B C E E' E''		
Unstable (1)		A B C D E E' E'' F G H	A B C E E' E''	A B C E E' E''	A B C E E' E''	A B C E E' E''
Unstable (2)		A B C E E' E''				
Unstable (3)		A B C E'	A B C E E' E''			

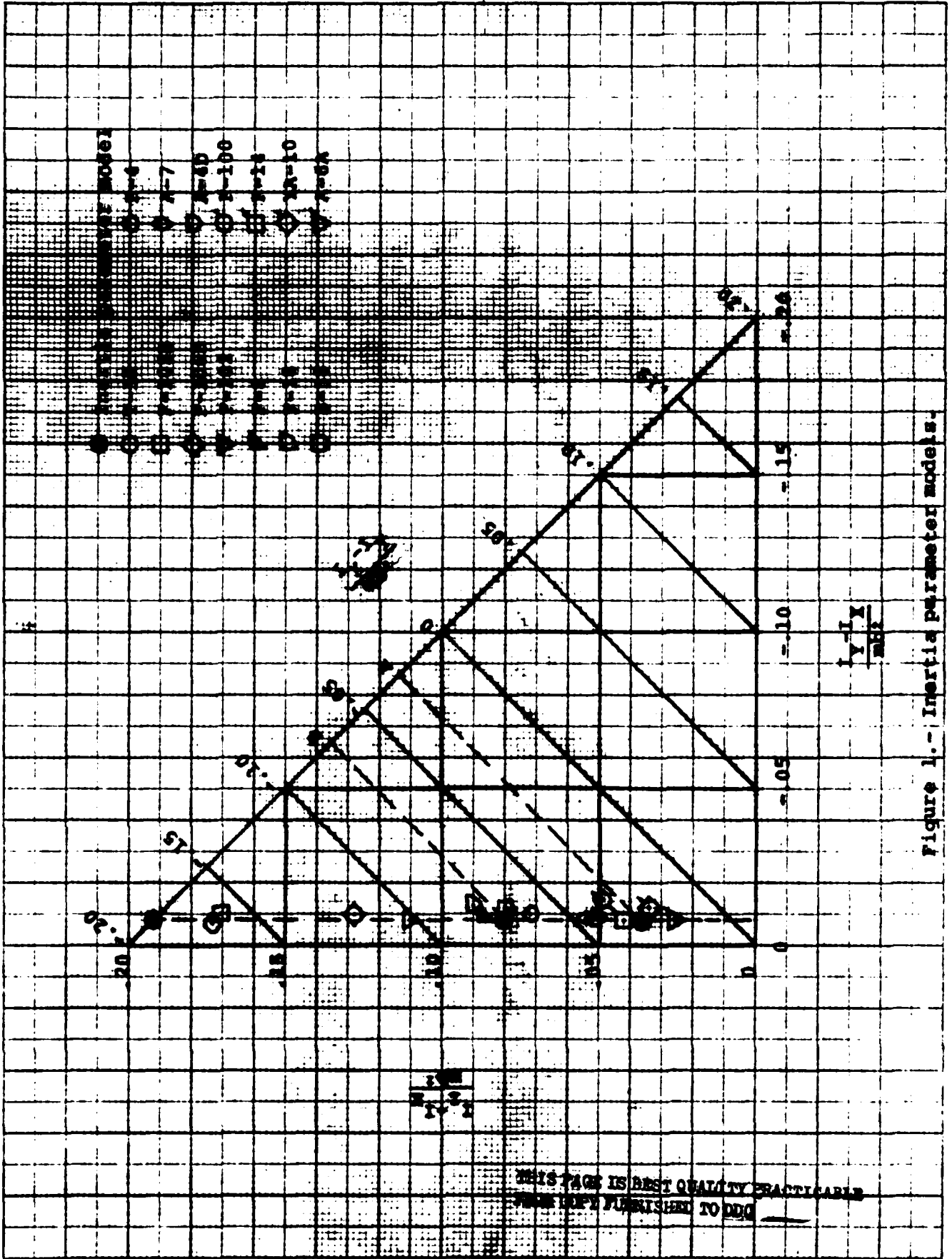
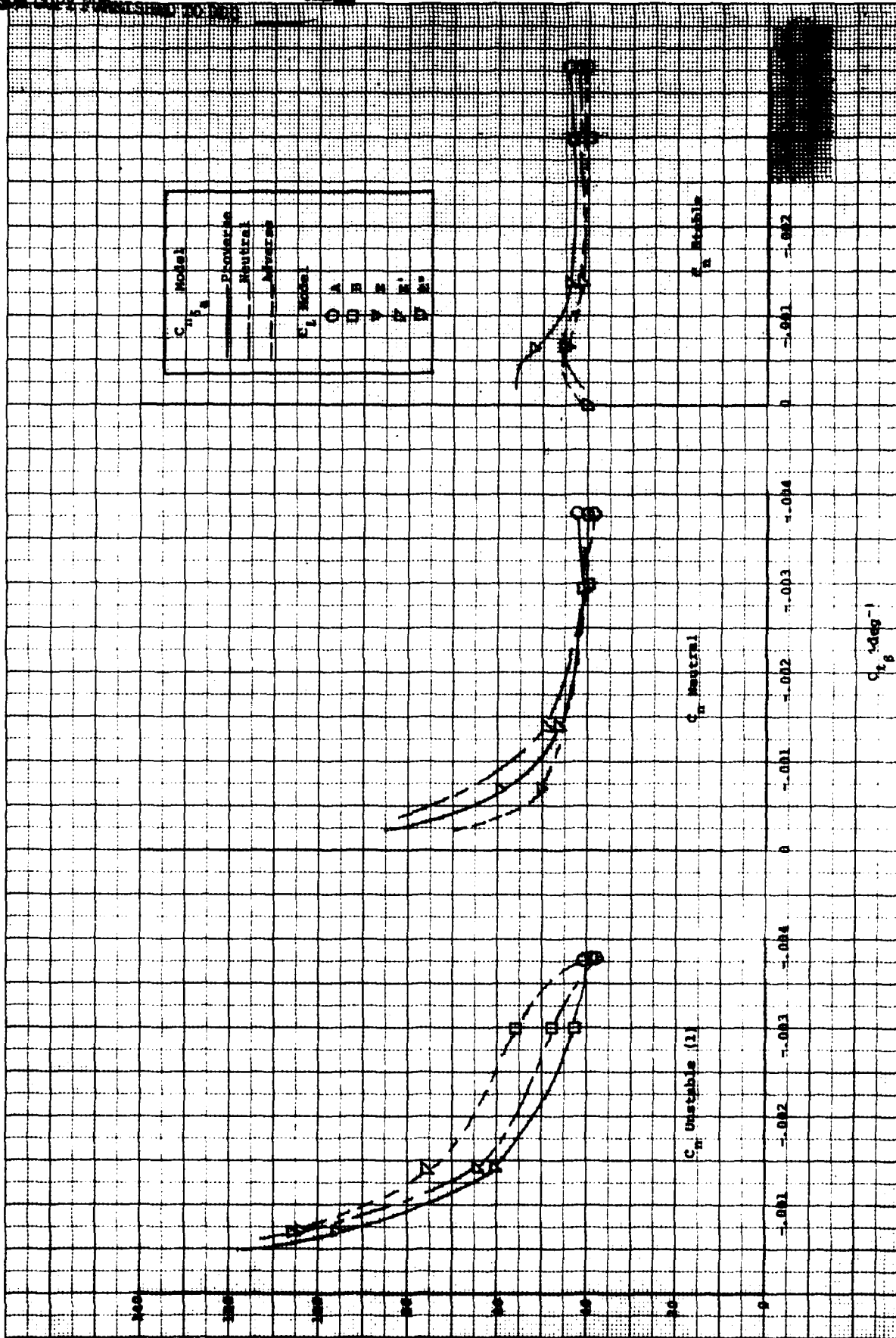


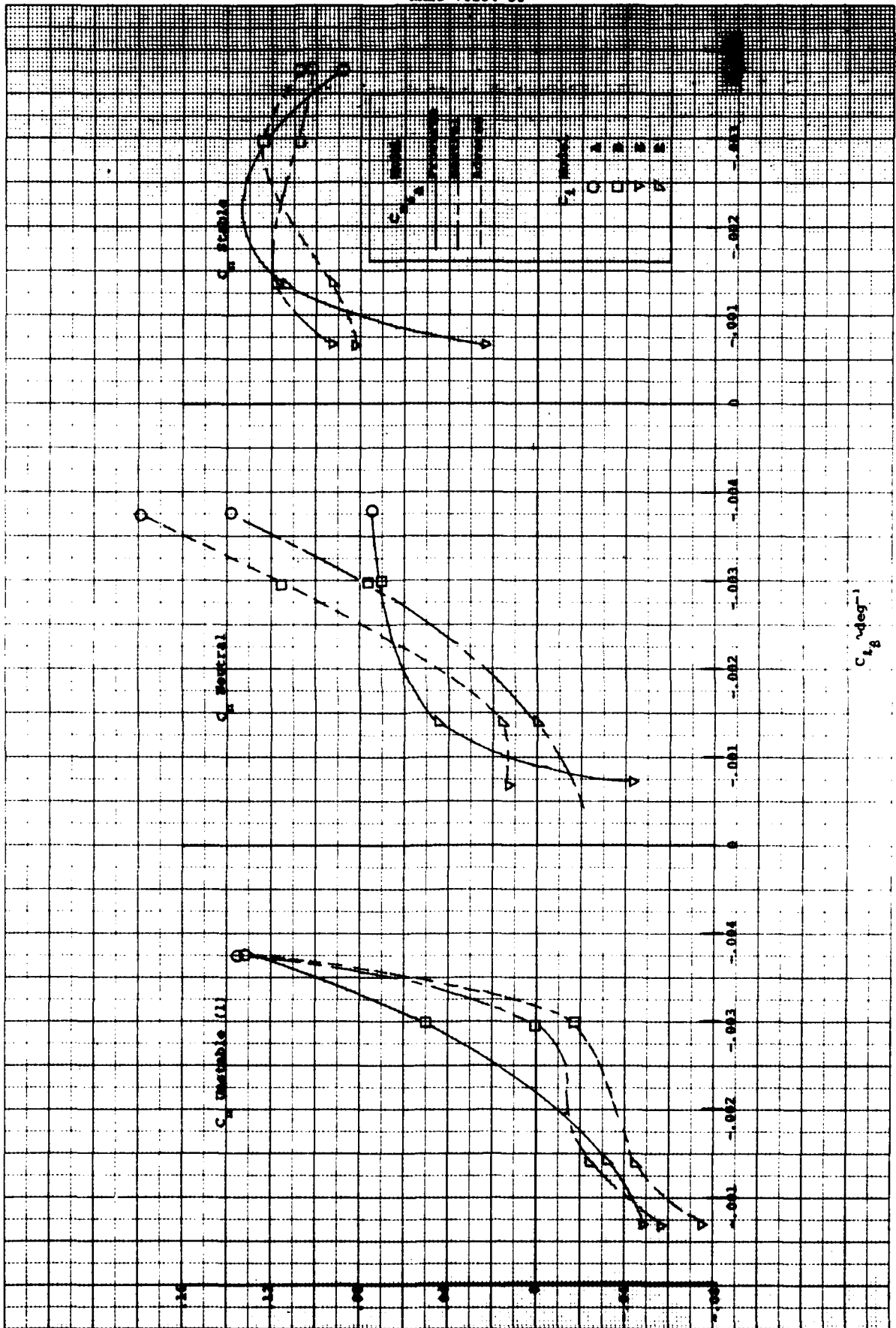
Figure 1.- Inertia parameter models.

THIS PAGE IS BEST QUALITY PRACTICABLE
 FROM COPY FURNISHED TO DDG

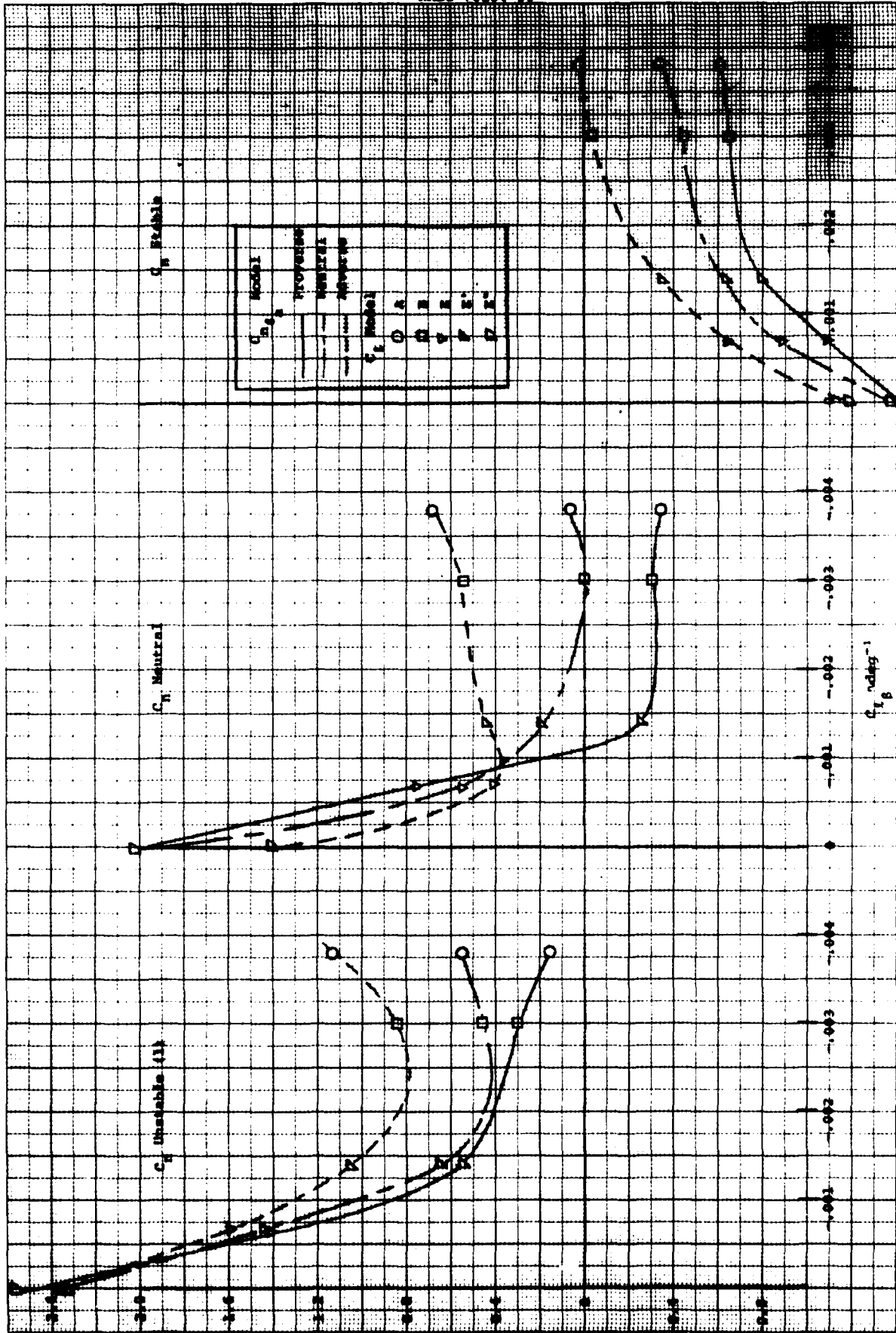


(a) Last alpha peak prior to lateral control removal as a function of the aerodynamic models.

Figure 2.- Design charts for determining departure susceptibility.



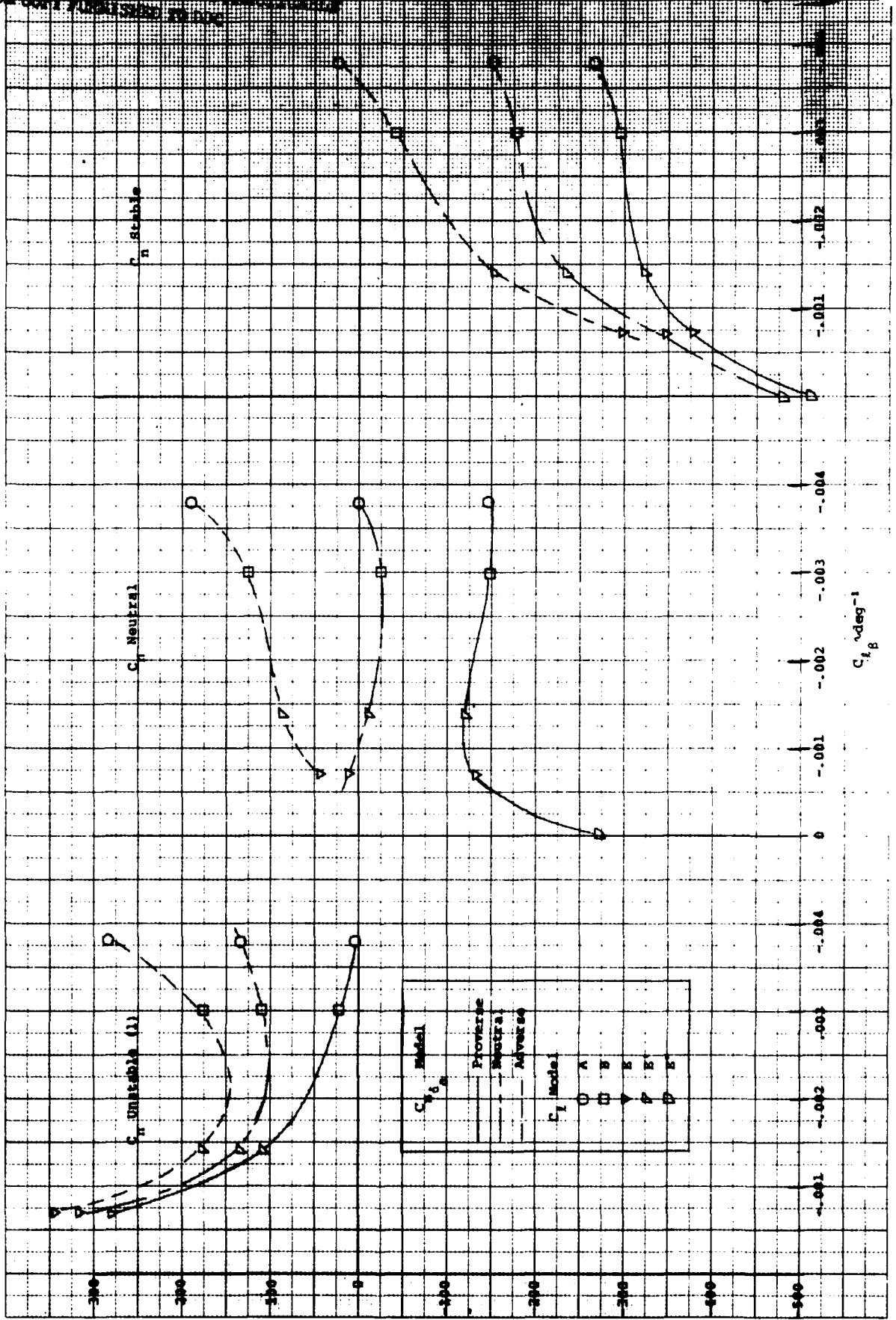
(b) Approximate second order damping ratio of alpha trace as a function of the aerodynamic models.
Figure 2.- Continued.



(c) Peak yaw rate as a function of the aerodynamic models.
Figure 2.- Continued.

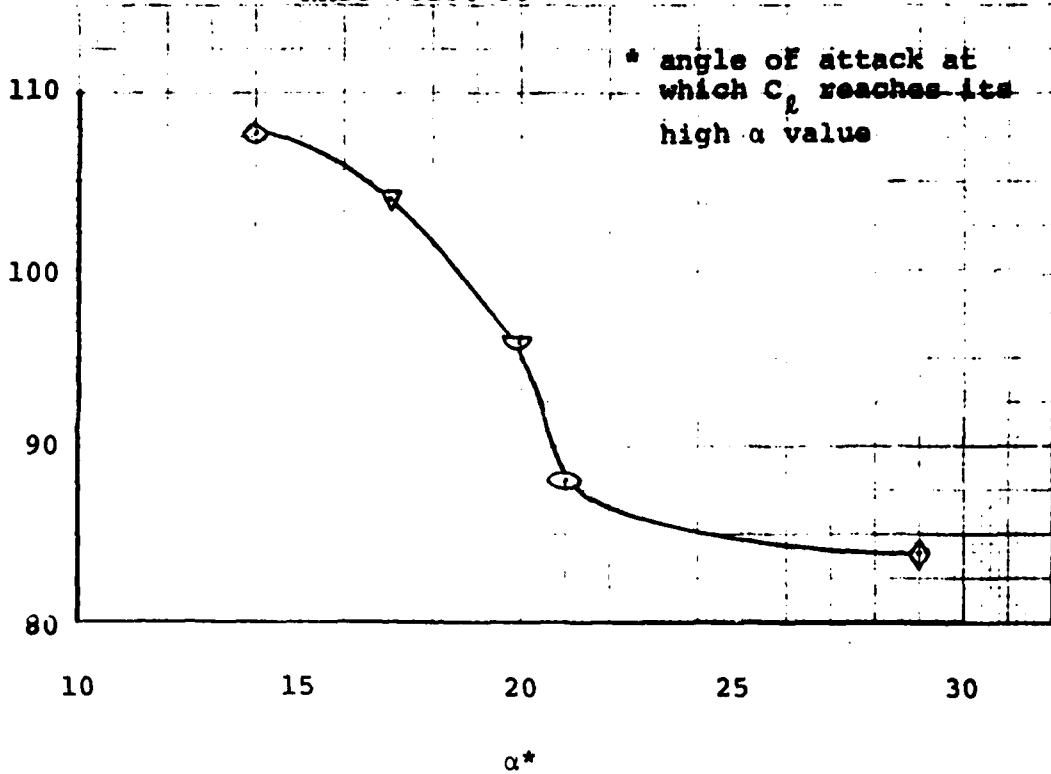
THIS PAGE IS BEST QUALITY PRACTICABLE
FROM COPY FURNISHED TO DDC

Peak yaw rate, rad/sec

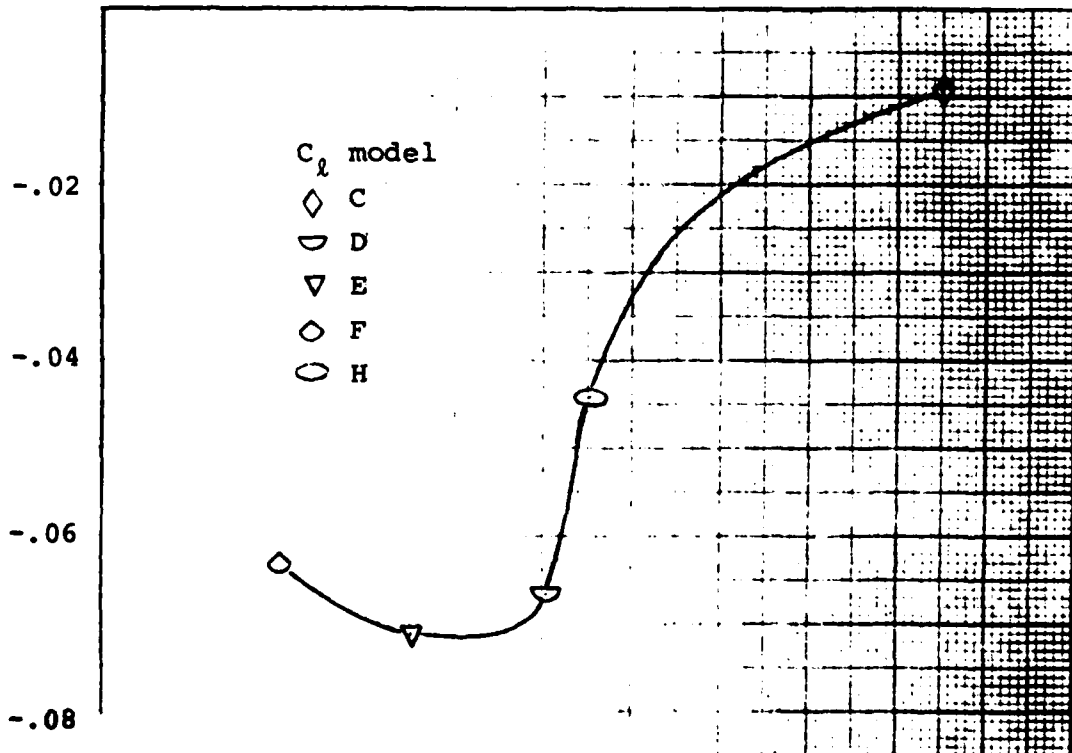


(d) Incremental peak bank angle reached at time lateral control removed.
Figure 2.- Concluded.

Last α peak prior to lateral control removal, deg

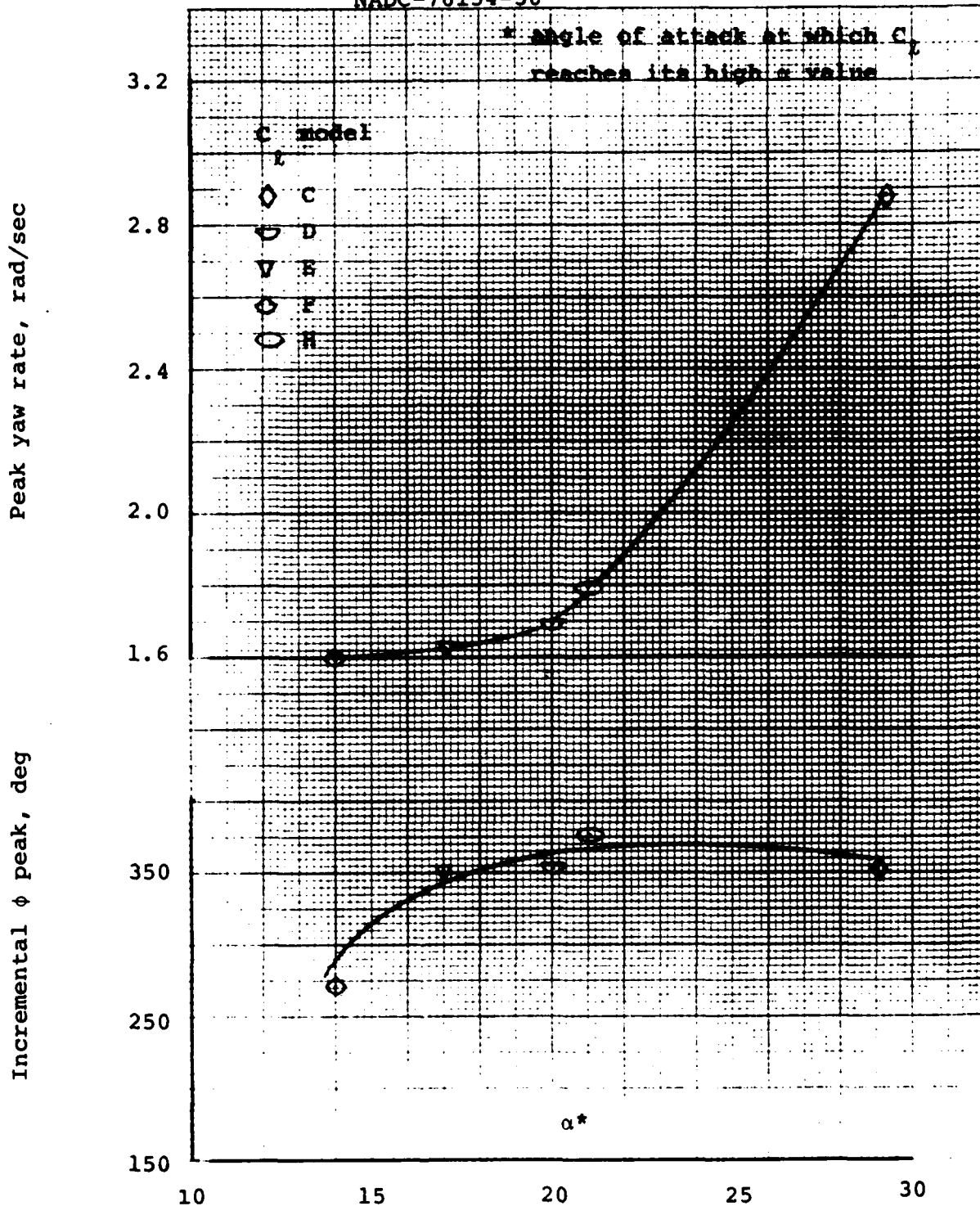


Approximate α damping ratio



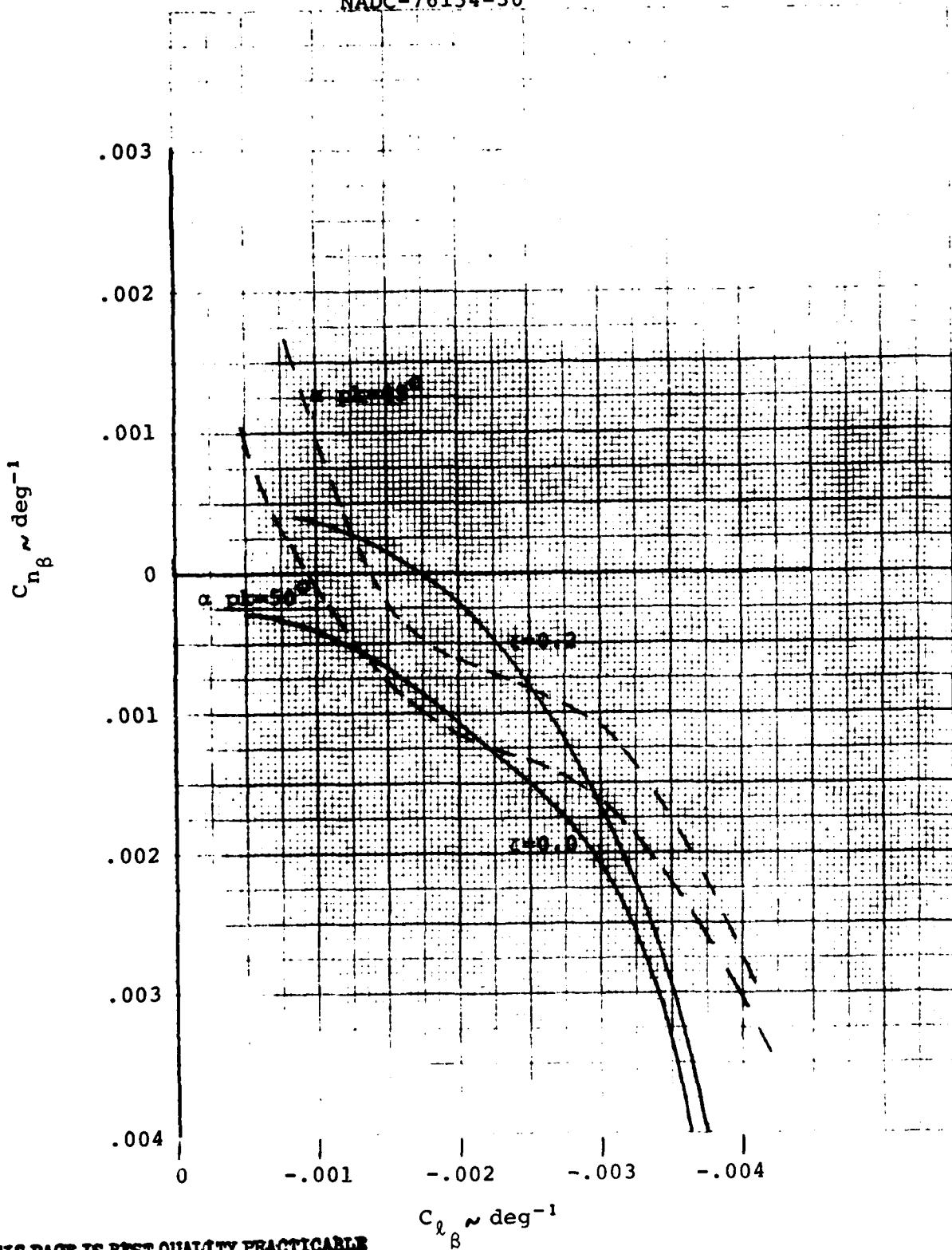
(a) Angle of attack time history trace parameters.

Figure 3.- Effect of the rate of onset in the loss of lateral stability on design chart information.



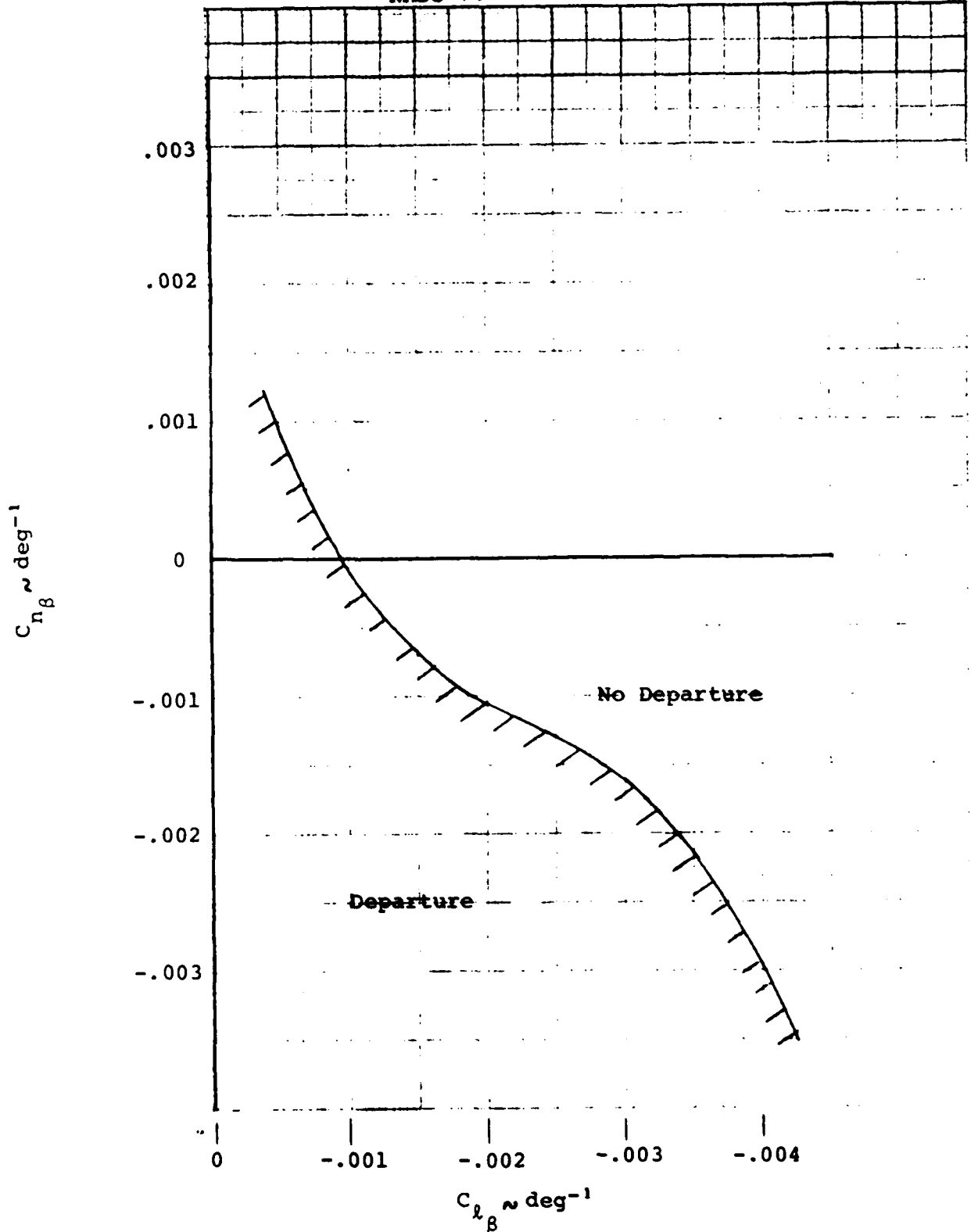
(b) Peak yaw rate and incremental peak bank angle reached at time lateral control removed.

Figure 3.- Concluded.



THIS PAGE IS BEST QUALITY PRACTICABLE
FROM COPY FURNISHED TO DDC

Figure 4.- Constant alpha peak and damping ratio curves derived from design charts as a function of lateral and directional stability for adverse $C_{n_{\delta_a}}$.



(a) Adverse $C_{n\delta_a}$

Figure 5.- Departure boundaries.

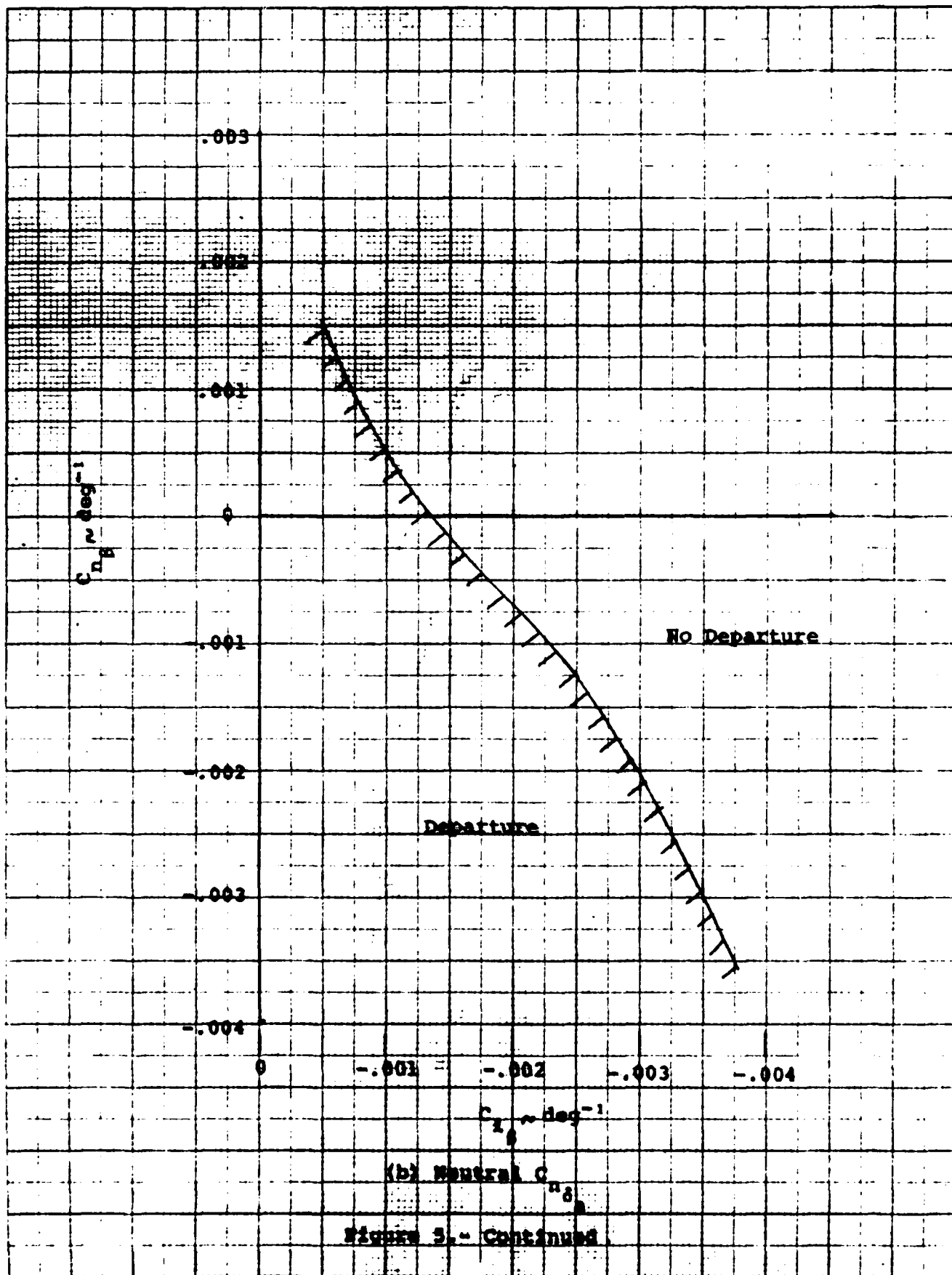


Figure 5.- Continued

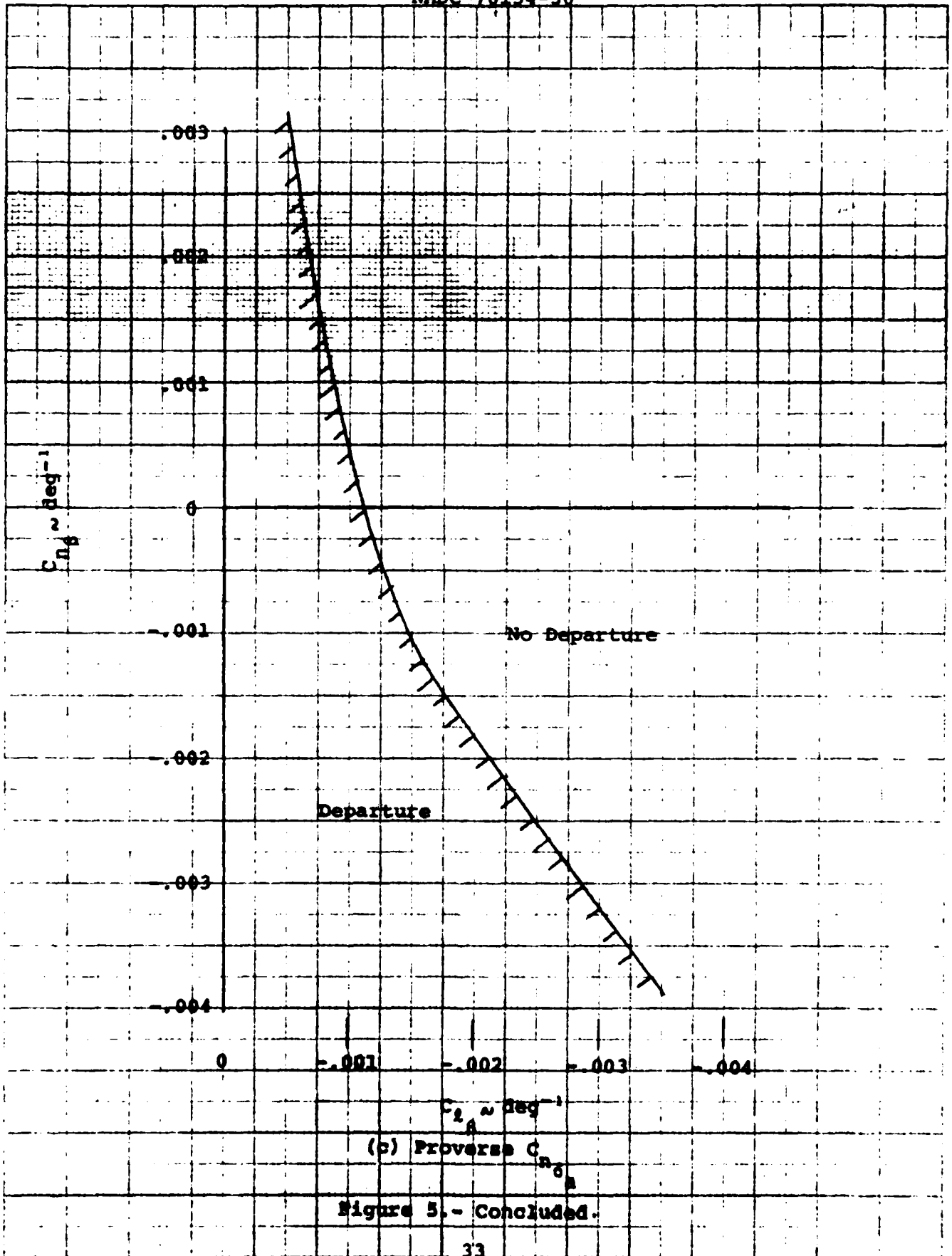
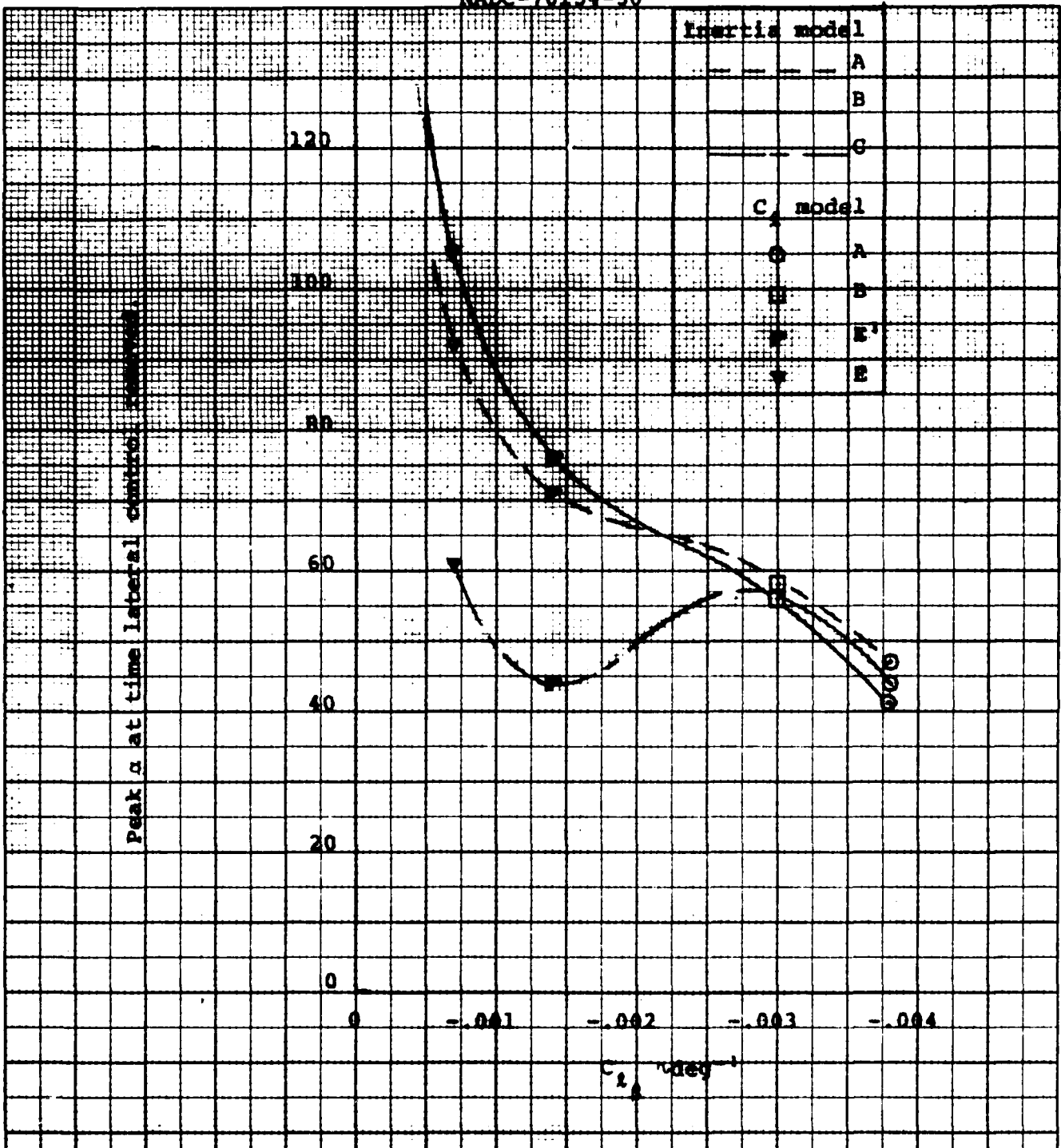
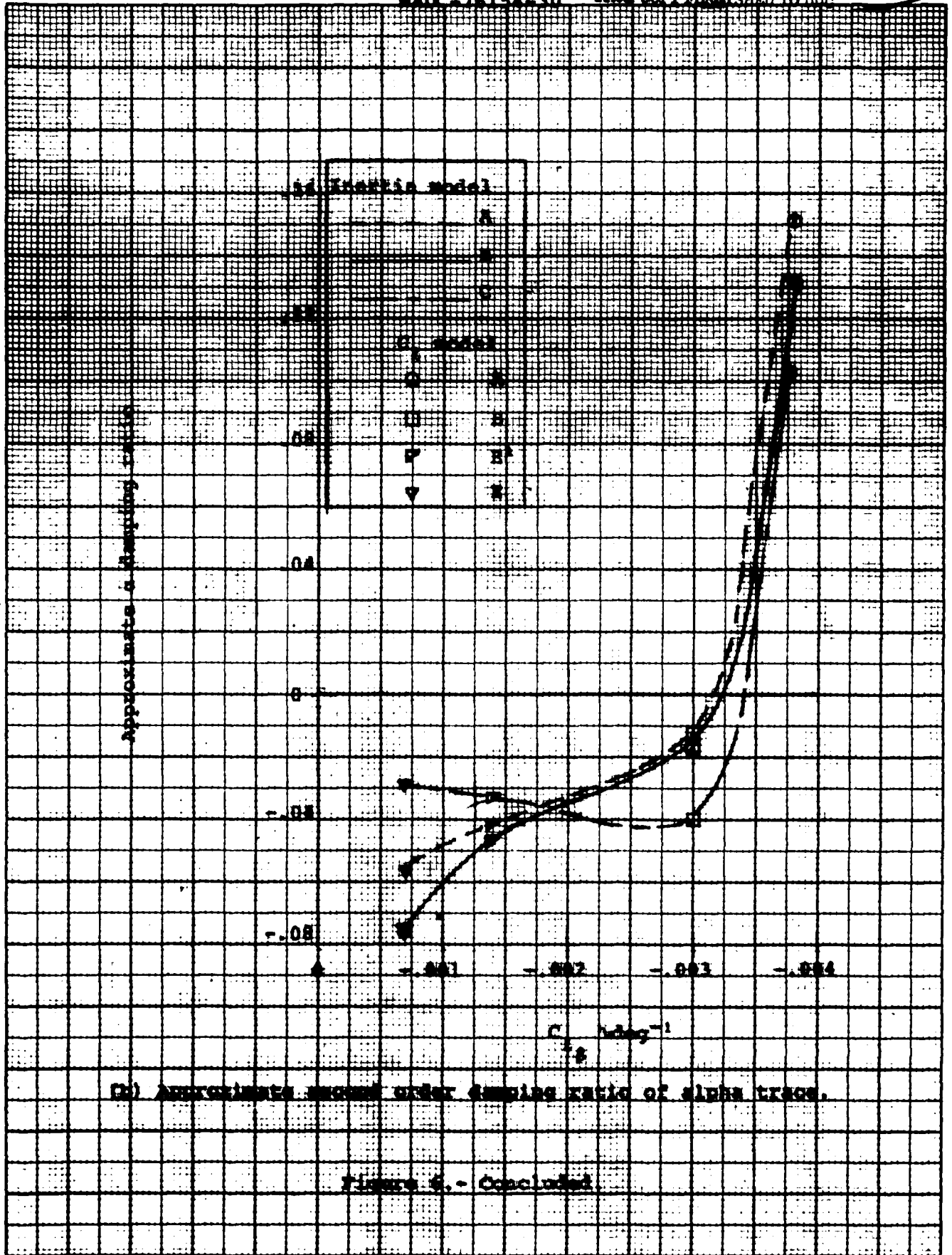


Figure 5.- Concluded.



(a) Peak alpha at time lateral control removed.

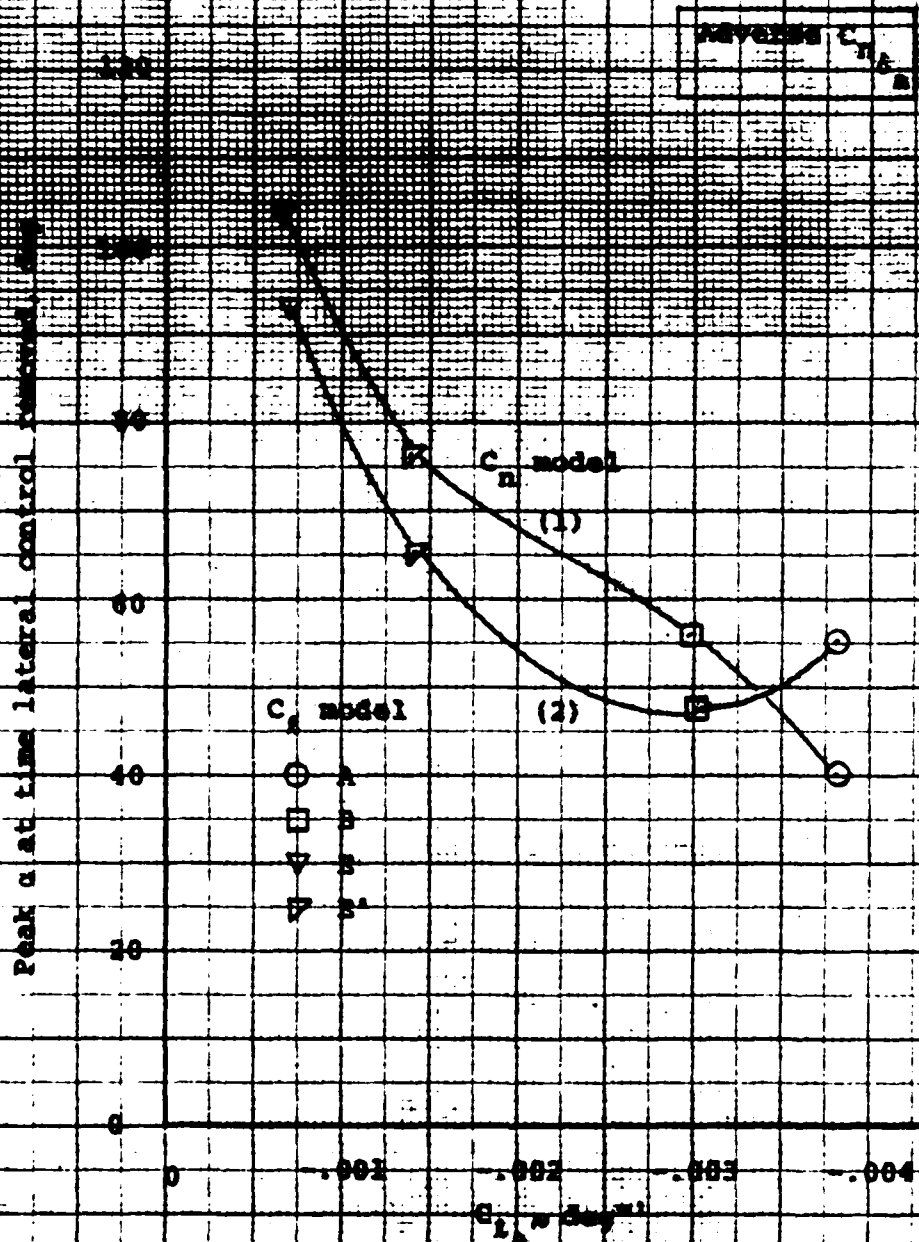
Figure 5. - Effect of inertia parameter models on design chart information.



(2) Approximate second order sampling ratio of alpha trace.

Figure 6.- Concluded

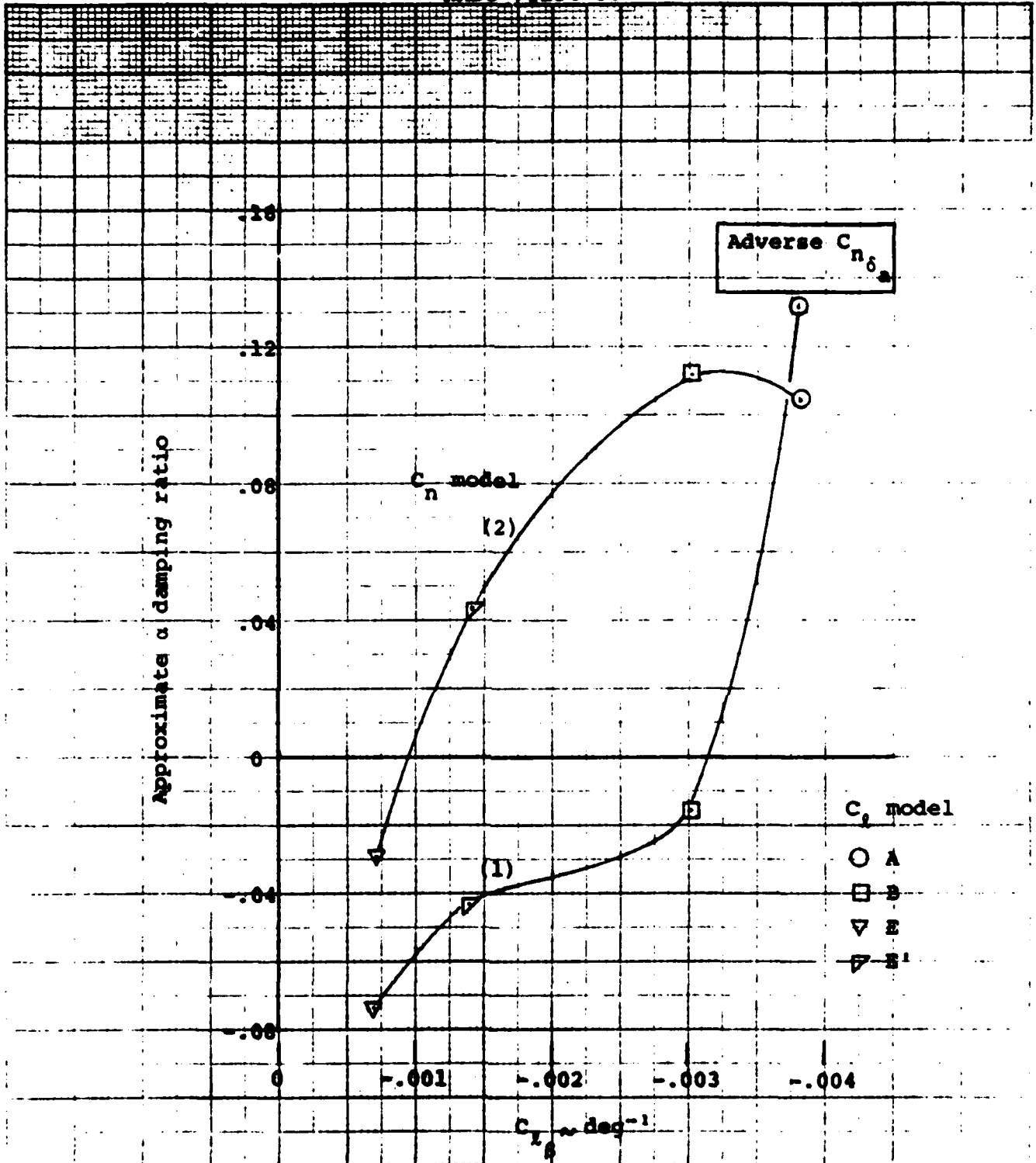
NW 80 03883 0 124J023



(a) Peak alpha at time lateral control removed.

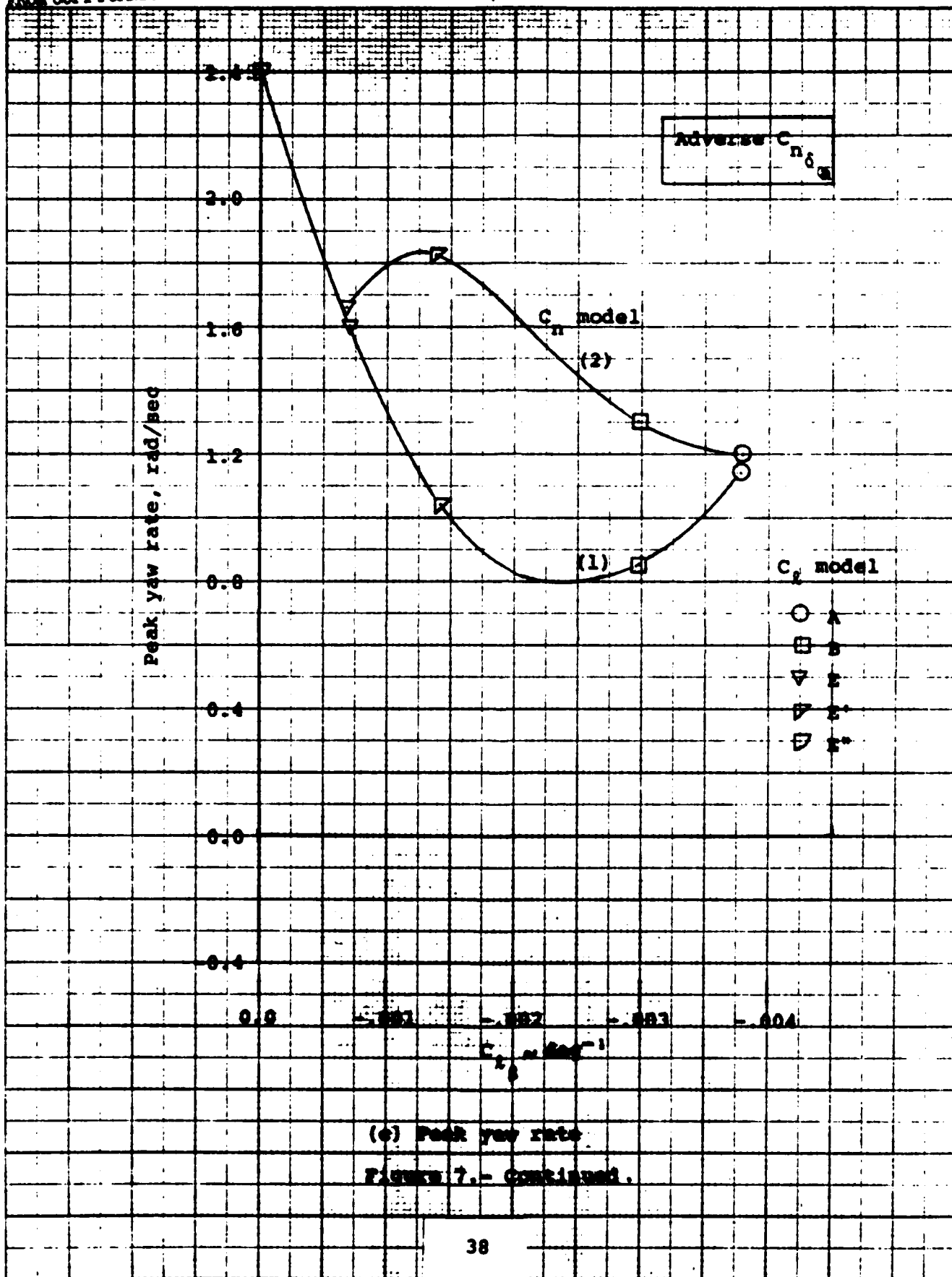
Figure 7. Effect of maintaining directional stability to a higher alpha on design chart information.

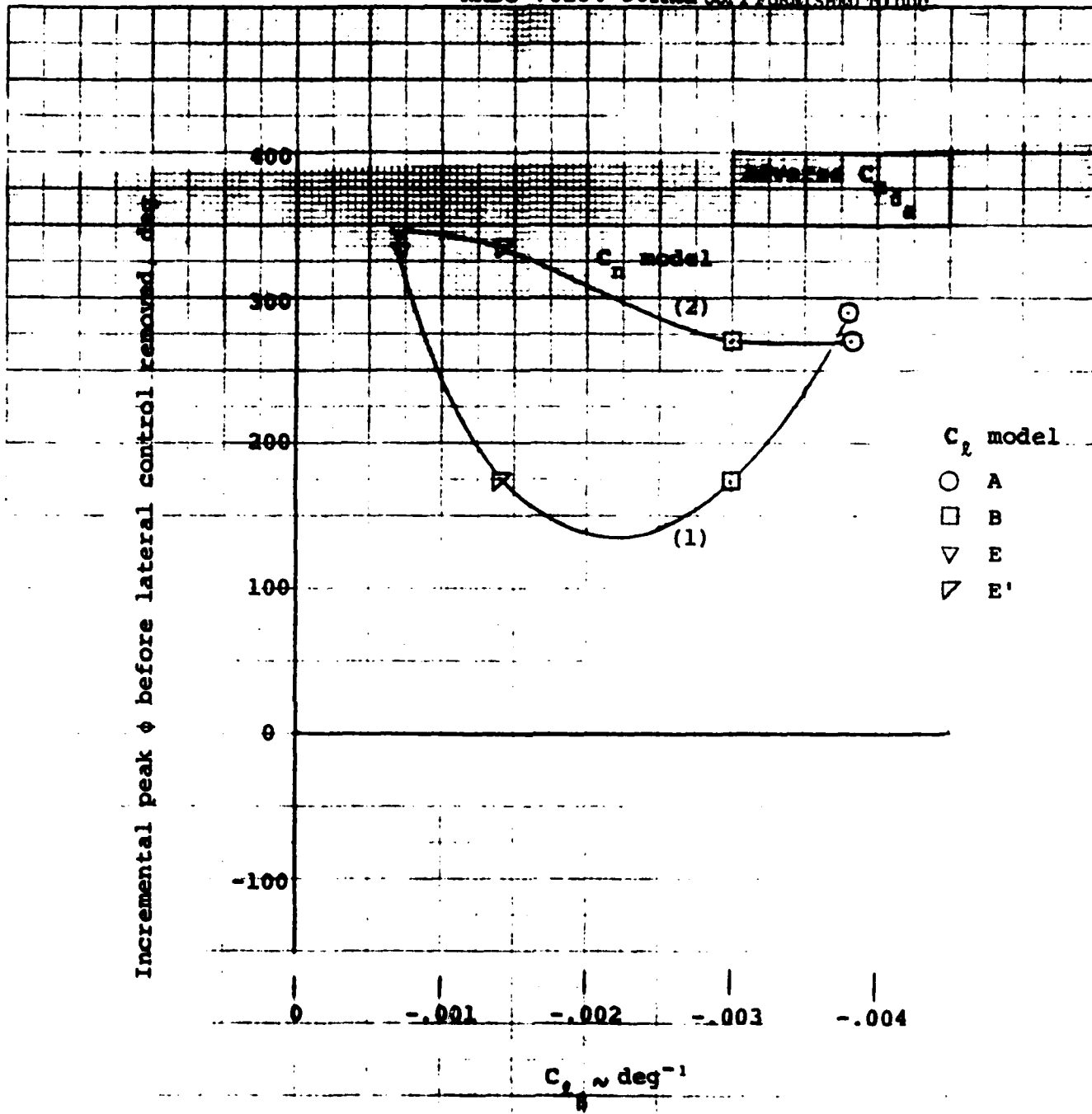
17 50 8321 4 11/60



(b) Approximate second order damping ratio of alpha trace.

Figure 7.- continued.





(d) Incremental peak bank angle reached at time lateral control removed.

Figure 7.- Concluded.

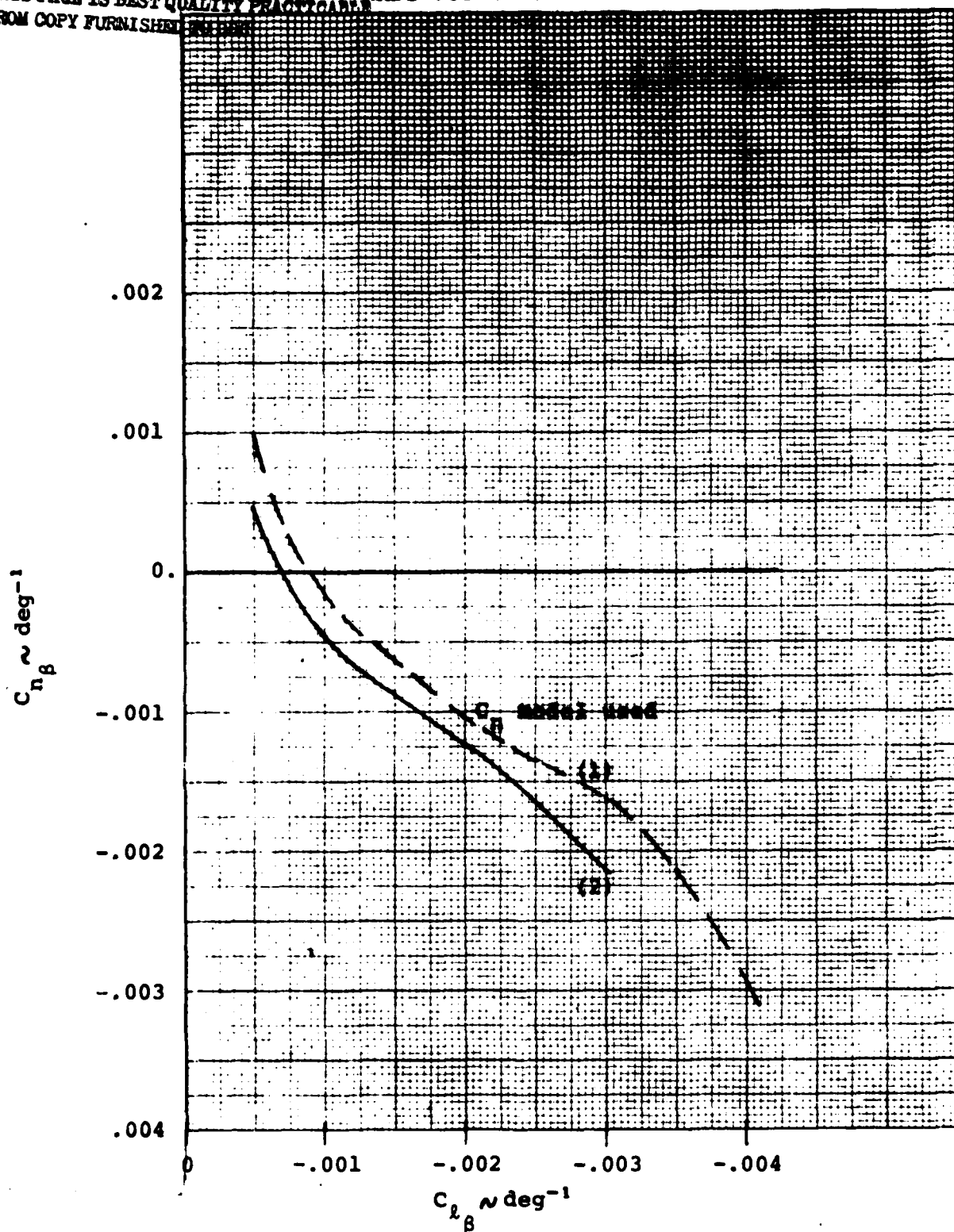


Figure 8.- Effect of maintaining directional stability to a higher alpha on departure boundary for adverse $C_{n\delta_a}$.

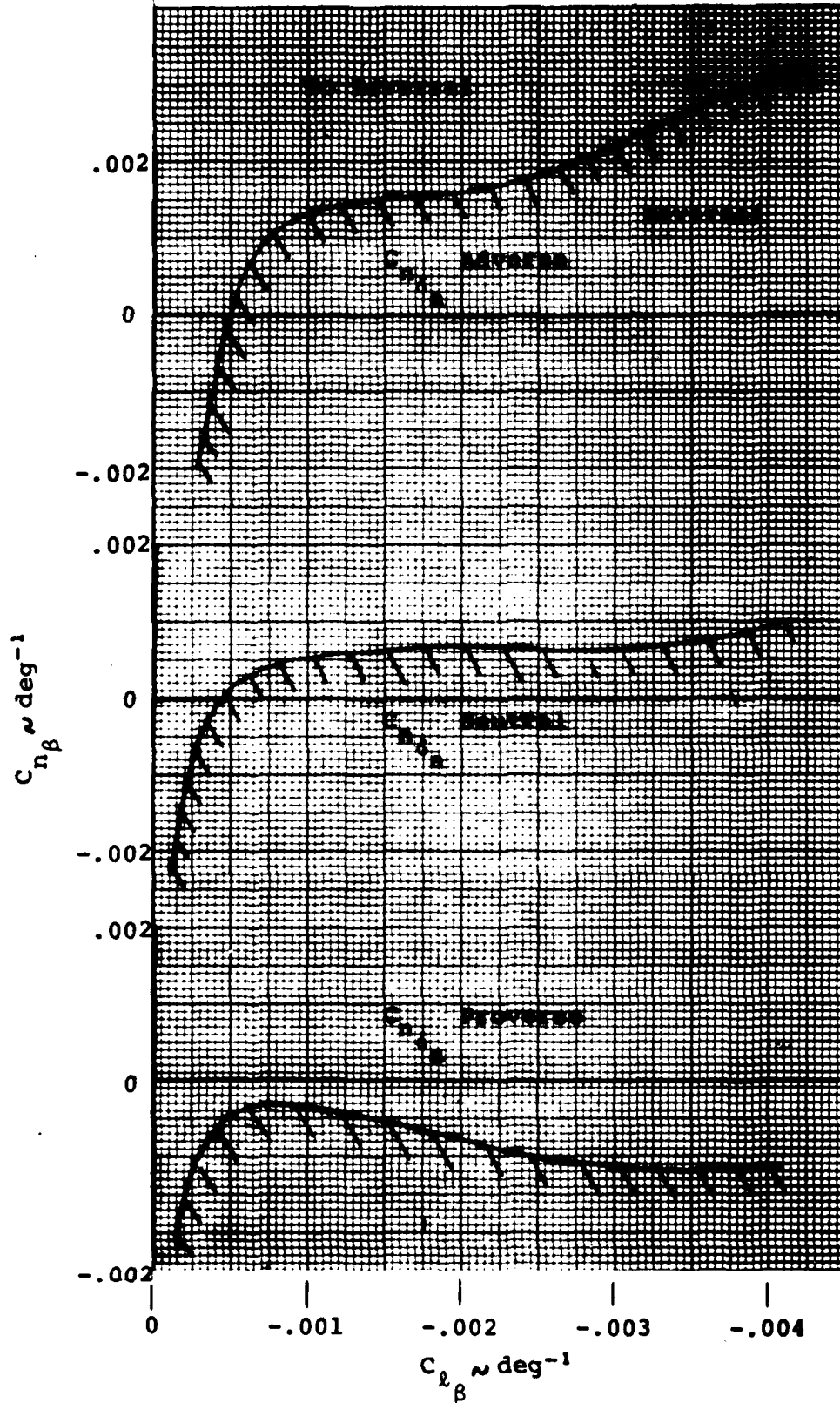


Figure 9.- Uncoordinated roll-reversal boundary.

APPENDIX A

The C_ℓ , C_n and $C_{n\delta_a}$ models investigated in this study, as well as a compilation of the airplane data upon which these models were based, are presented in this appendix. Also shown are the aerodynamic derivatives which were held constant during the investigation.

C_ℓ and C_n values obtained during high Reynolds number wind tunnel tests of various fighter type configurations are presented in figures A1 and A2, respectively, as a function of angle of attack for 10 degrees of sideslip. These are sample plots of the collected data employed to construct the C_ℓ and C_n models.

Figures A3 and A4 show the selected C_ℓ models as a function of angle of attack for 10 and 25 degrees of sideslip, respectively. C_ℓ is zero throughout the angle-of-attack range for zero sideslip and is assumed to remain constant with sideslip for sideslip angles greater than 25 degrees.

C_n models are shown in figures A5 and A6 for 10 and 25 degrees of sideslip, respectively, as a function of angle of attack. As for the C_ℓ models, C_n is zero for zero sideslip, and the level is constant for sideslip angles greater than 25 degrees.

The $C_{n\delta_a}$ models are shown in figure A7 to be a function of angle of attack and represent typical levels of proverse and adverse yaw realized with fighter airplane configurations.

The aerodynamic parameters which were not varied during the study are presented in figures A8 through A24. As shown,

normal and axial coefficients, figures A8 through A11, were programmed as functions of angle of attack, sideslip angle and longitudinal control deflection. The pitching moment coefficient, figures A12 and A13, was also programmed as a function of angle of attack, sideslip angle and control deflection. The pitching moment is typical of what might be found on those fighter airplanes which are statically stable in pitch throughout the angle-of-attack range. The side force coefficient, C_y , also programmed as a function of α , β and longitudinal control deflection, is shown in figures A14 and A15. The lateral control derivatives were programmed as functions of angle of attack and lateral and longitudinal control deflections. The longitudinal control deflection dependence is due to the fact that many current fighter configurations utilize differential elevator deflection for lateral control. The $C_{l_{\delta_a}}$ model is shown in figures A16 and A17, and the $C_{y_{\delta_a}}$ model is shown in figures A18 and A19. The dynamic derivatives, C_{n_p} , C_{m_q} , etc., are shown in figures A20 through A24; each is a function of angle of attack and represents characteristic values for fighter type airplanes.

K&E
MEMBER OF ENGINEERING CO. AND ARCHITECTS
10 X 10 TO 1/8" INCH

10 1351

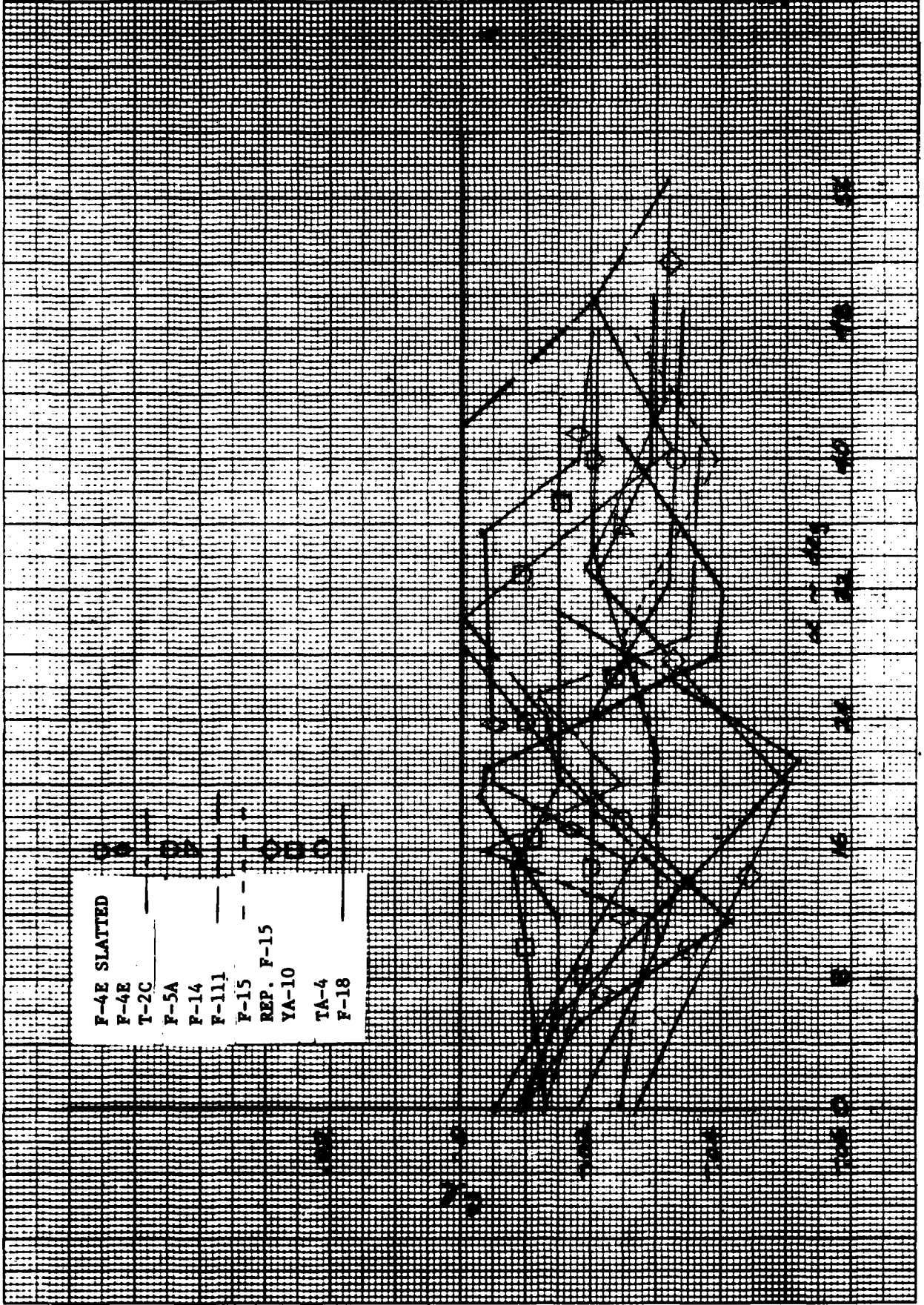


Figure A1.- Rolling moment coefficient as a function of angle of attack for various airplanes. $\beta = 10$ deg.

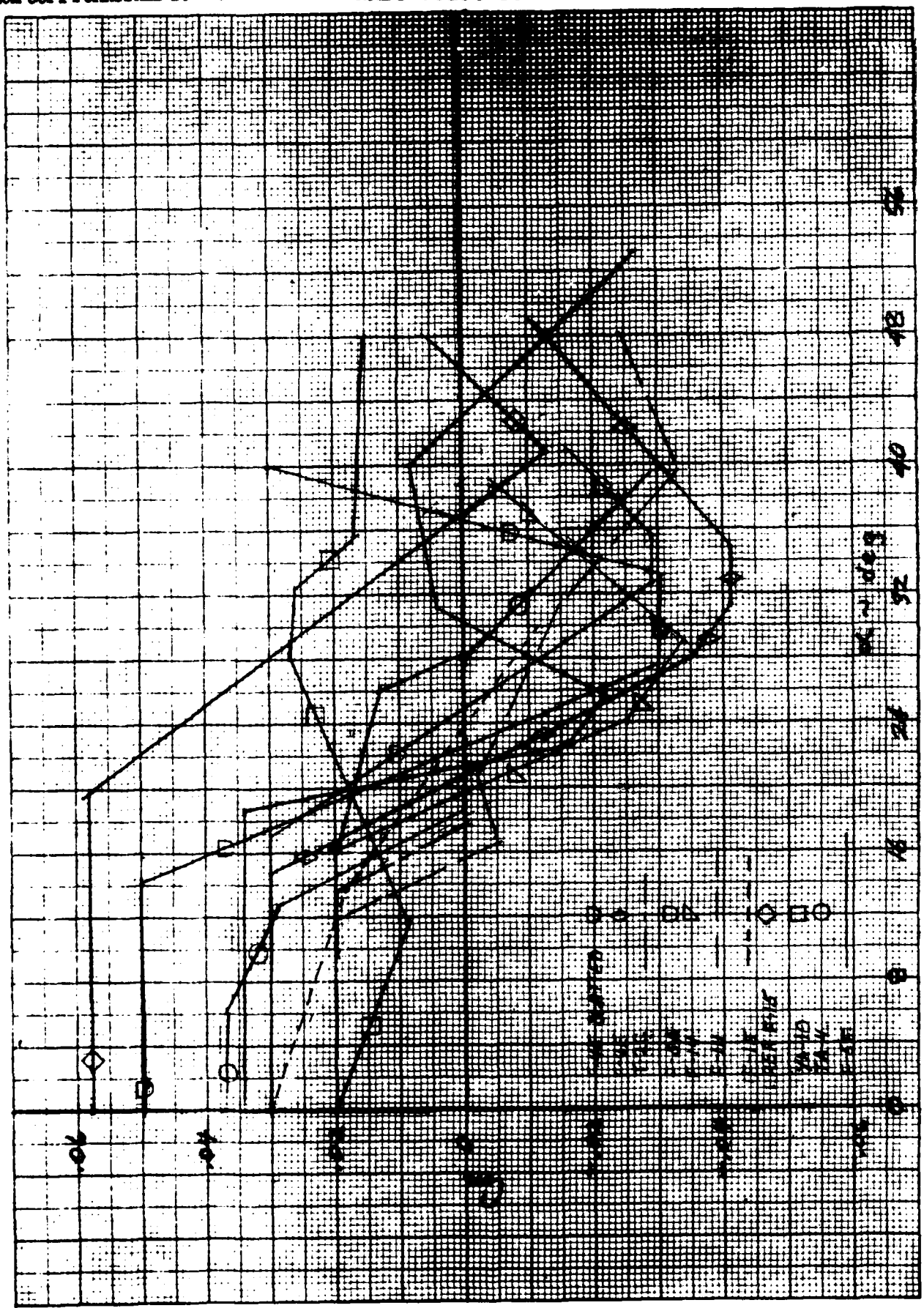


Figure A2.- Yawing moment coefficient as a function of angle of attack for various airplanes. $\beta = 10$ deg.

EUBENE DIETZGEN CO.
MADE IN U. S. A.

NO. 340A-10 1/2 DIETZGEN GRAPH PAPER
10 X 10 PER HALF INCH

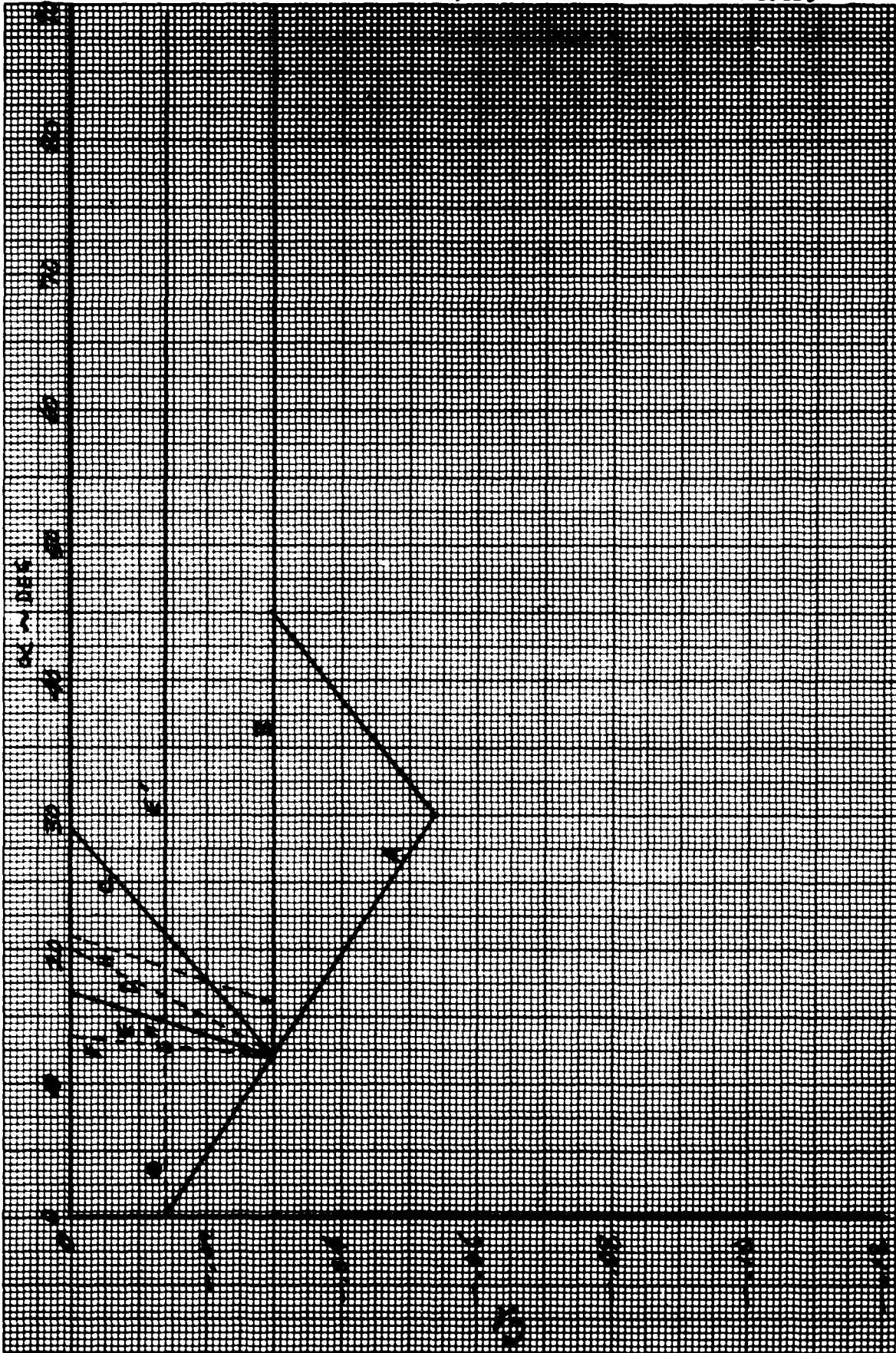


Figure A3.- Rolling moment coefficient models for $\beta = 10$ deg.

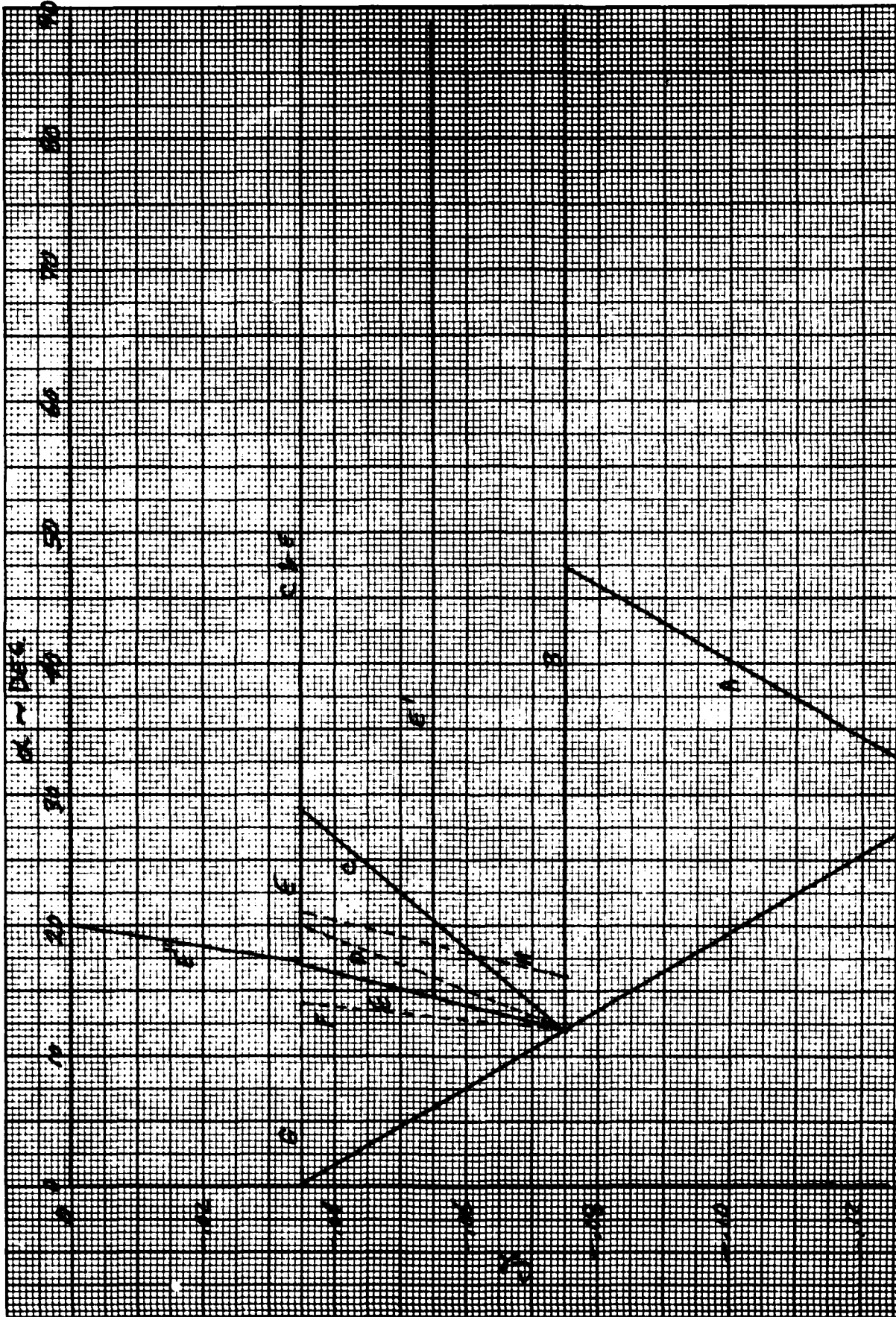


Figure A4.- Rolling moment coefficient models for $\beta = 25$ deg.

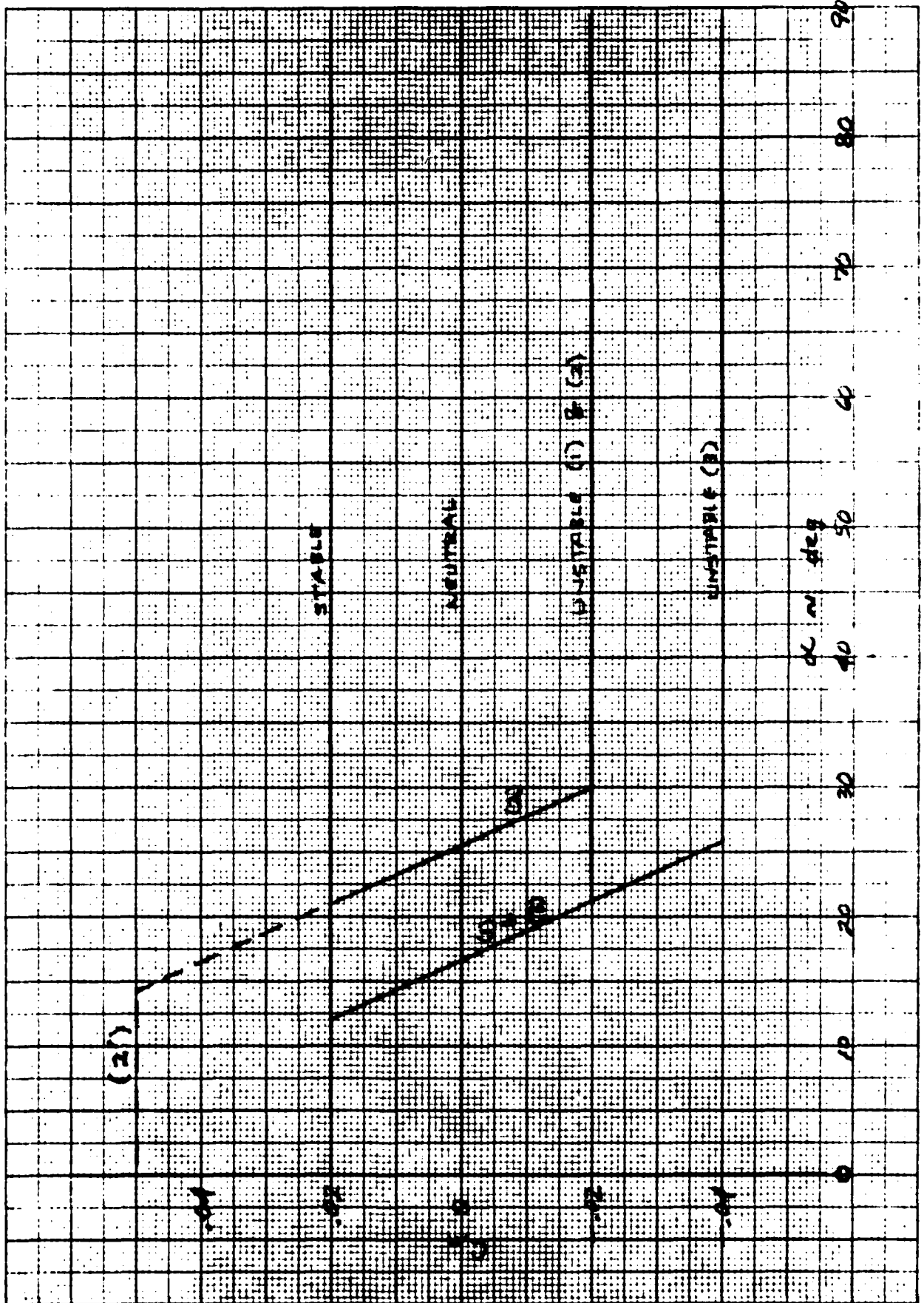


Figure A5.-Yawing moment coefficient models for $\beta = 10^\circ$.

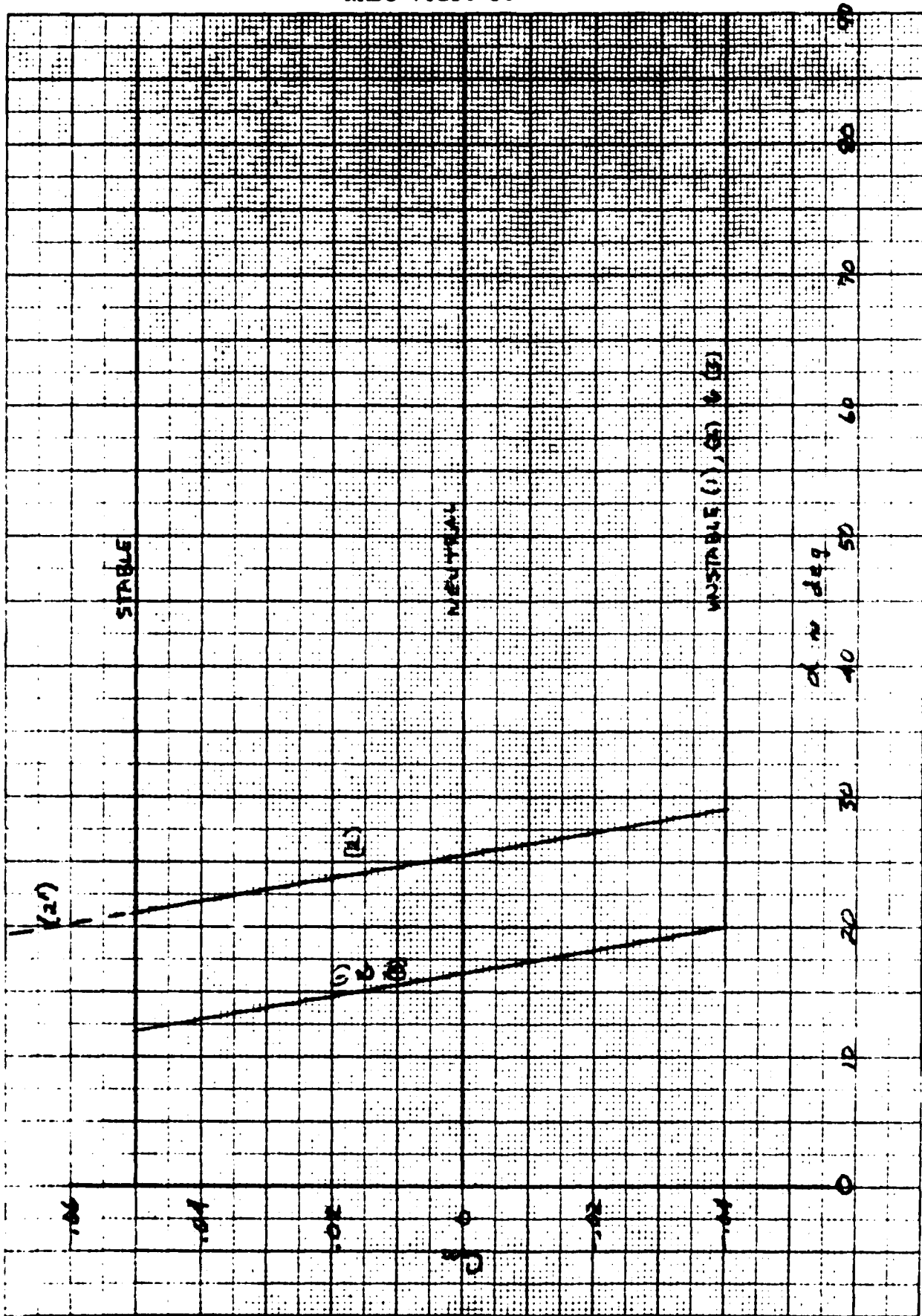


Figure A6.- Yawing moment coefficient models for $\beta = 25$ deg.

KOE 10 X 10 TO 1/4 INCH 46 1323
7 X 10 INCHES
HEUPPEL & BERBER CO.

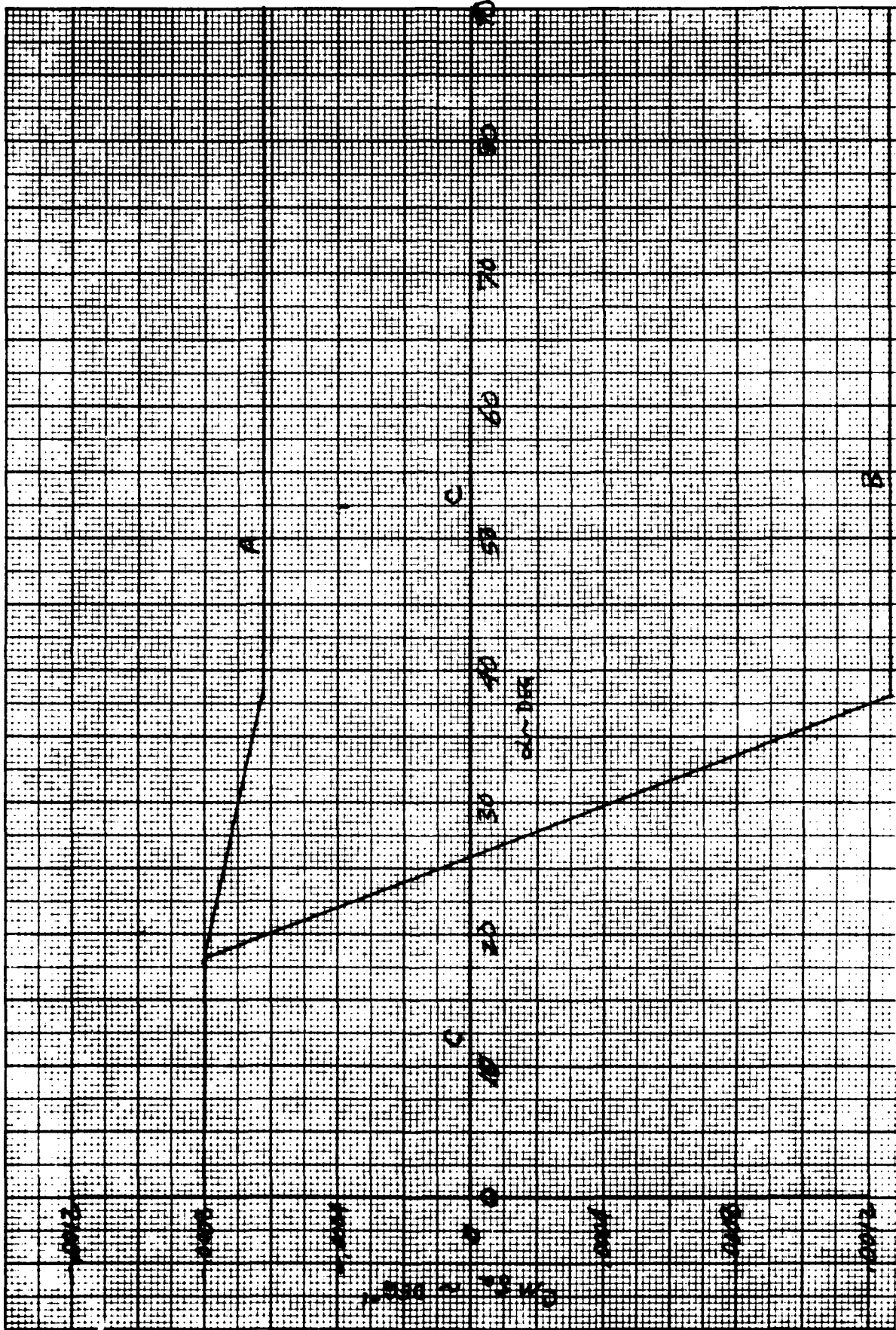


Figure A7.- Yawing moment due to lateral control derivative models.

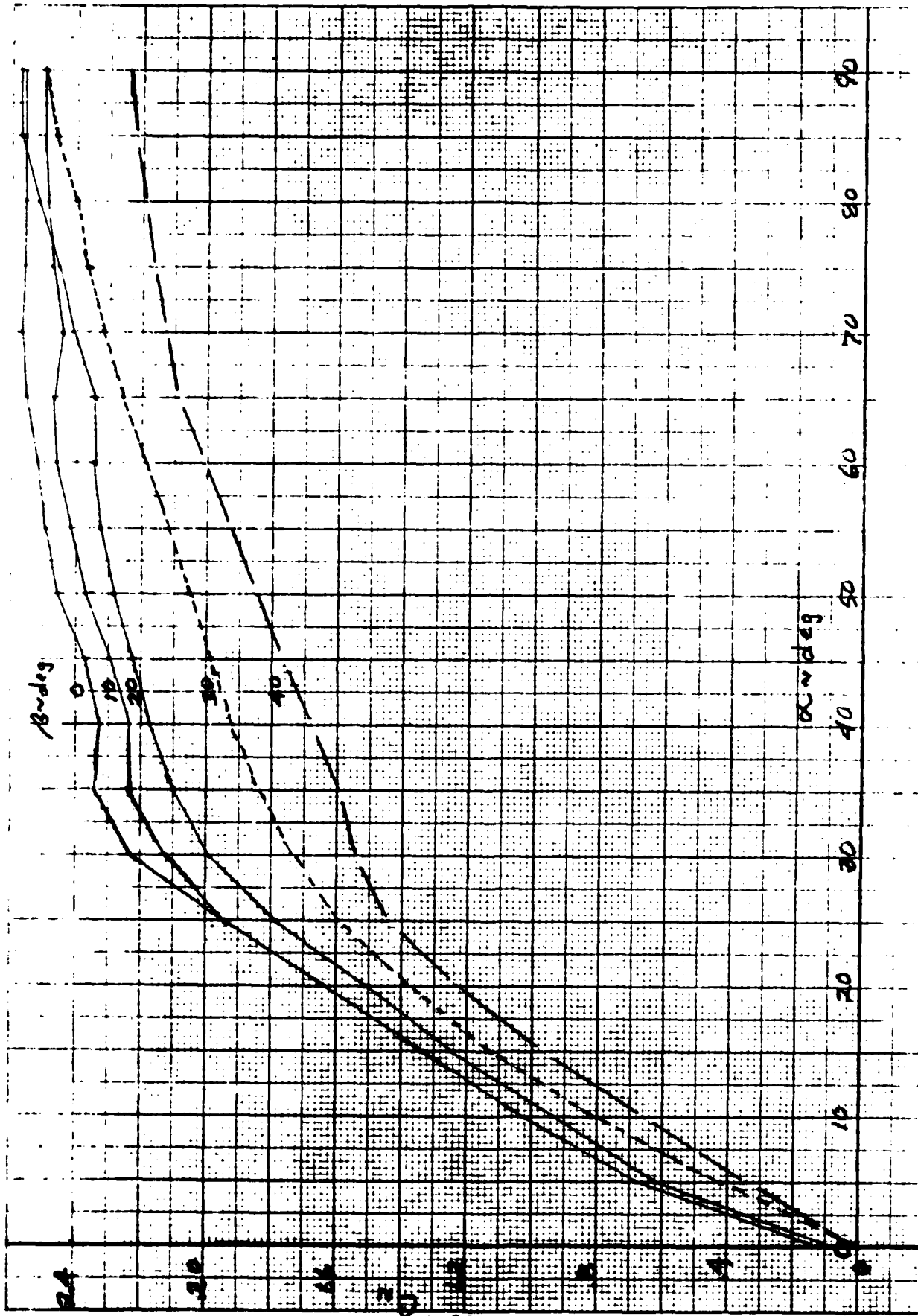


Figure A8.- Normal force coefficient as a function of angle of attack and sideslip angle. $i_s = 0$ deg.

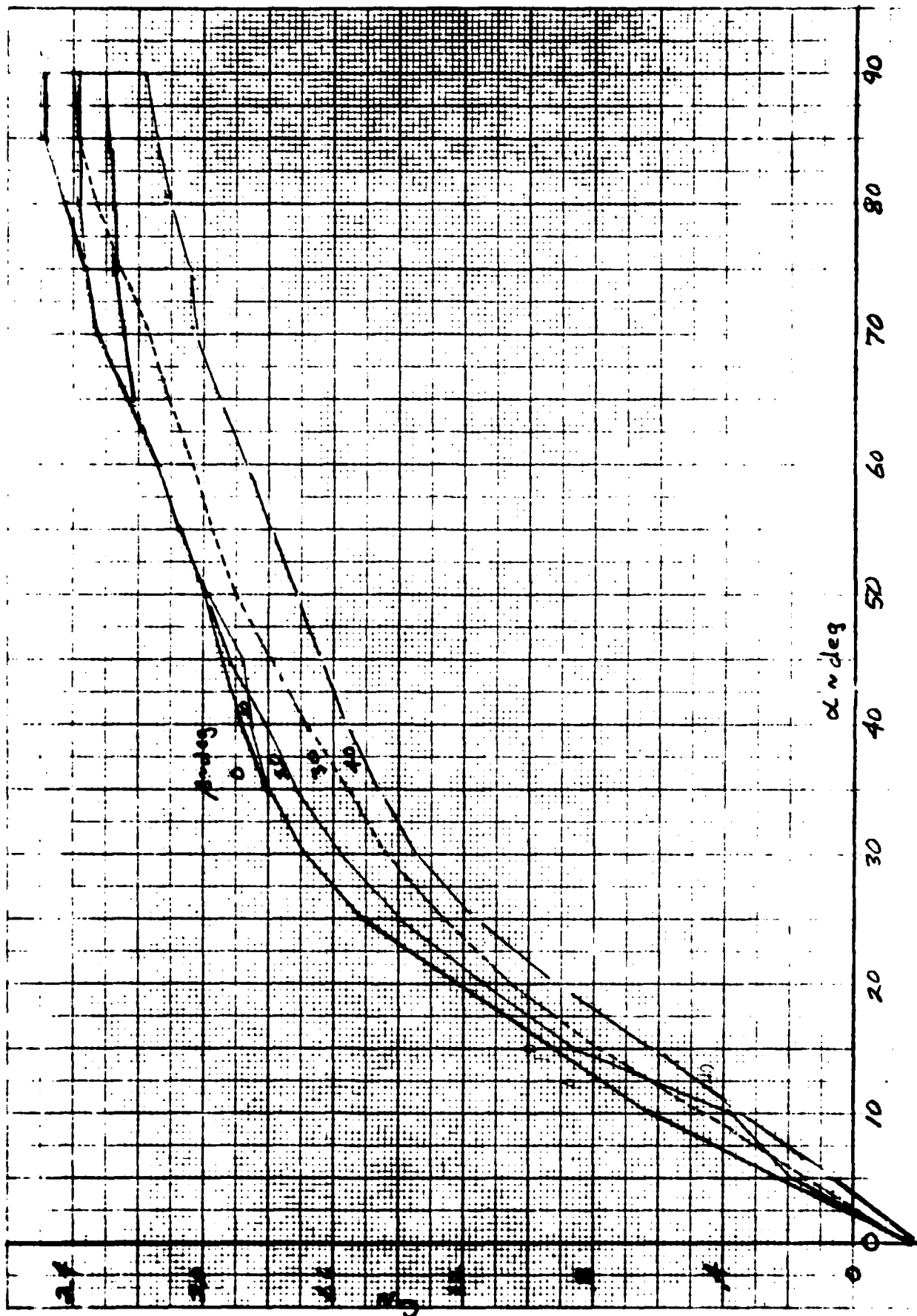


Figure A9.-Normal force coefficient as a function of angle of attack and sideslip angle. $i_s = -30$ deg.

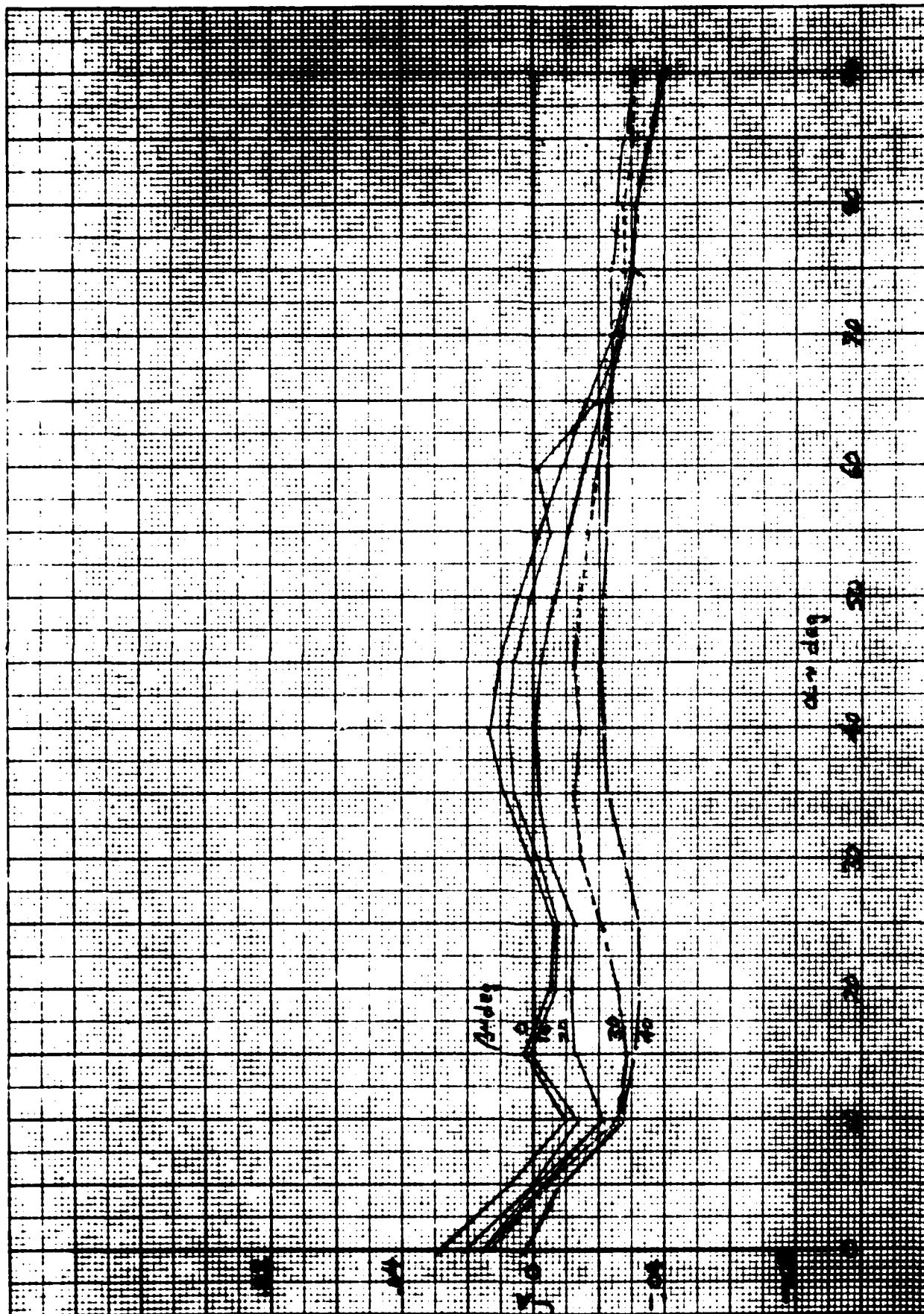


Figure A10.- Axial force coefficient as a function of angle of attack and sideslip angle. $i_s = 0$ deg.

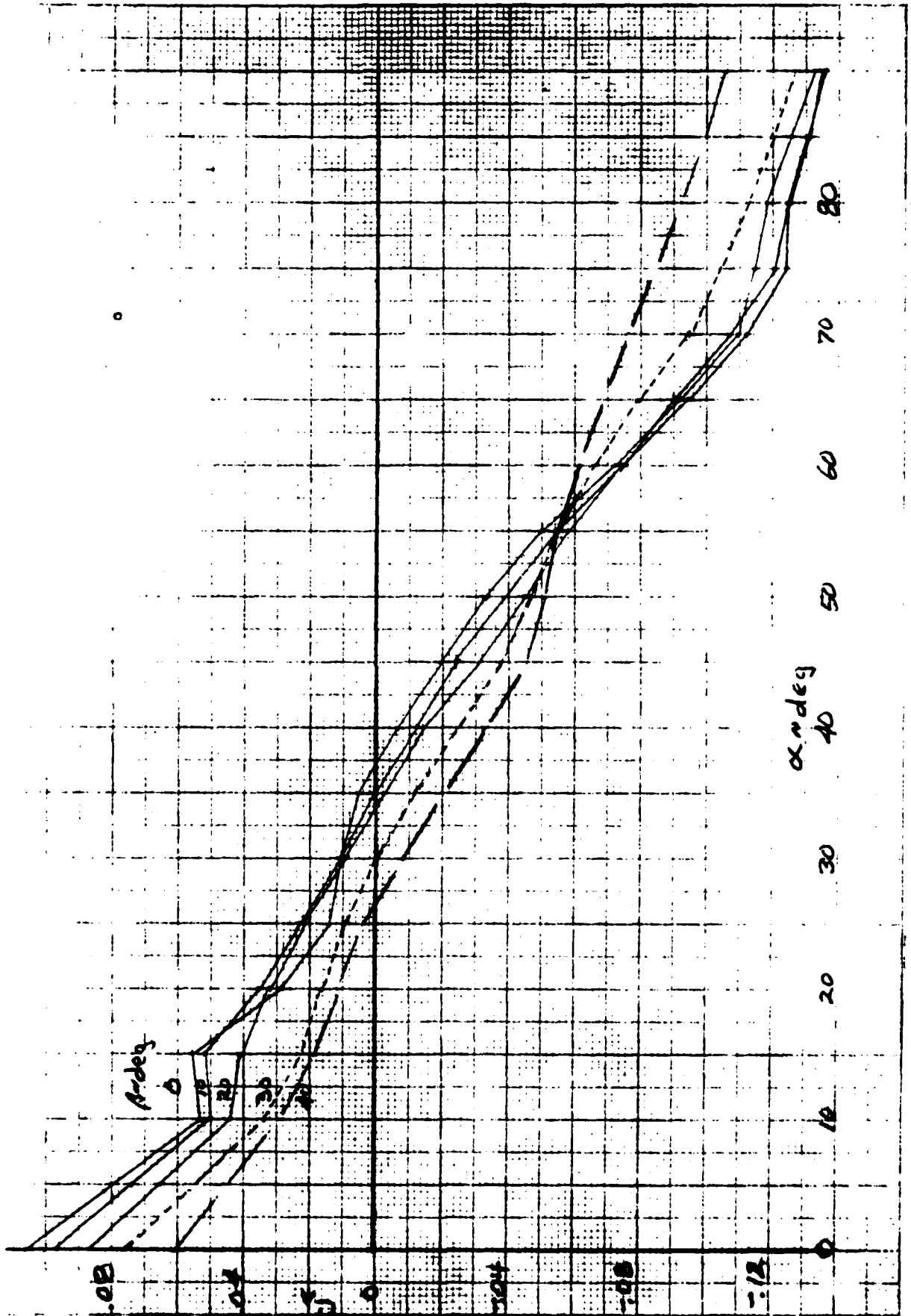


Figure All.- Axial force coefficient as a function of angle of attack and sideslip angle. $i_s = -30$ deg.

THIS PAGE IS BEST QUALITY PRACTICABLE
FROM COPY FURNISHED TO DDG

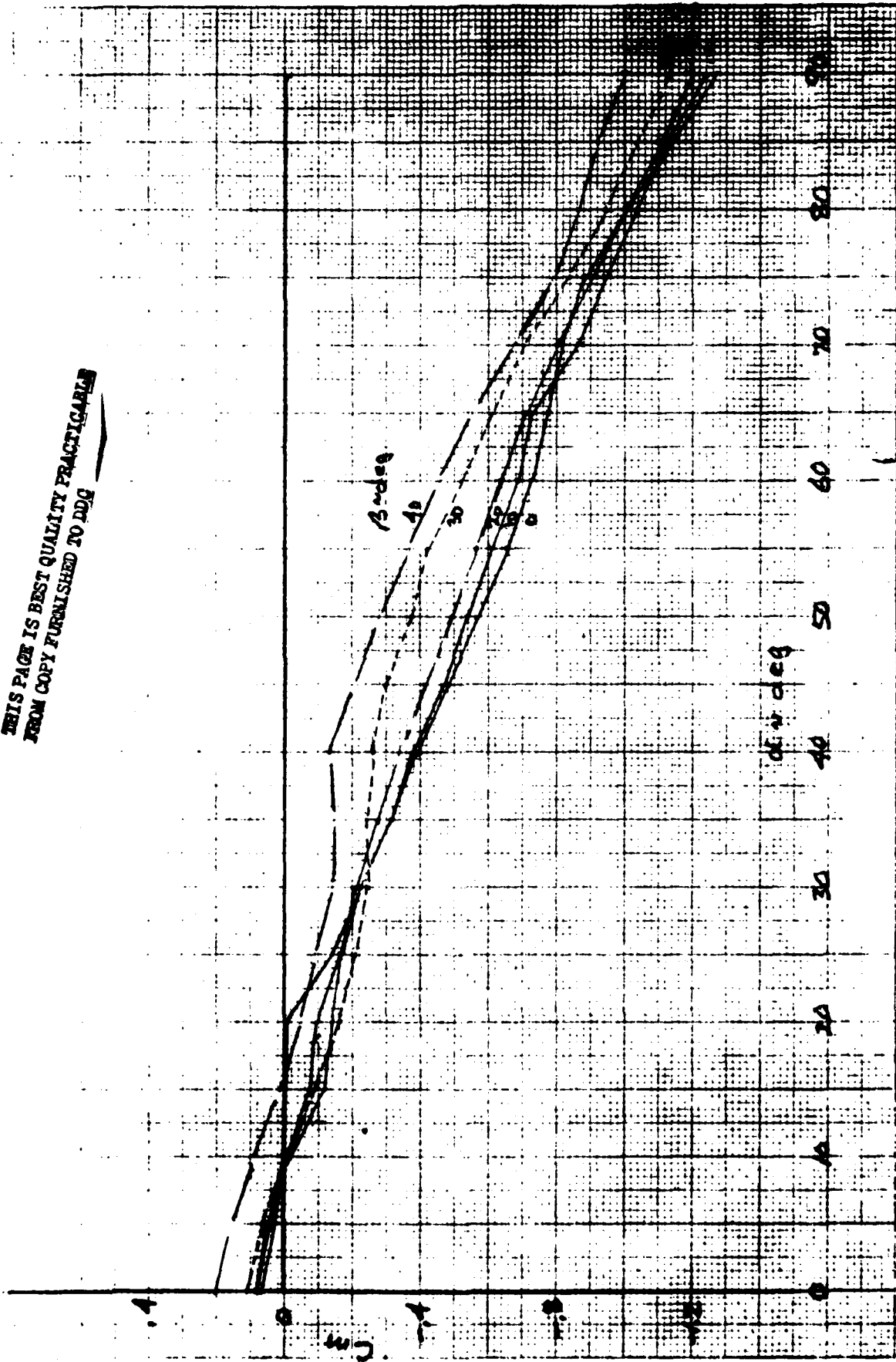


Figure A12.- Pitching moment coefficient as a function of angle of attack and sideslip angle. $i_s = 0$ deg.

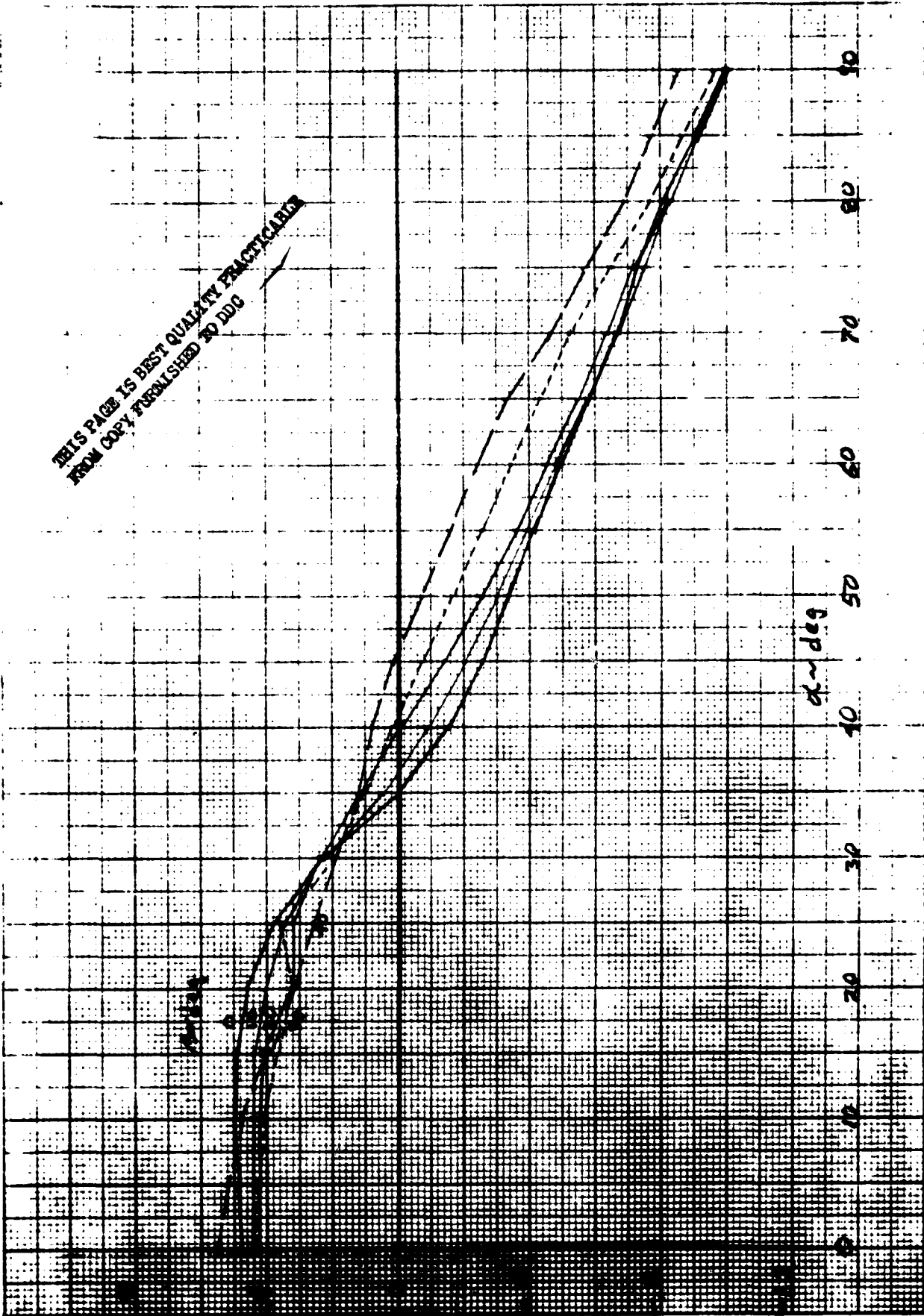
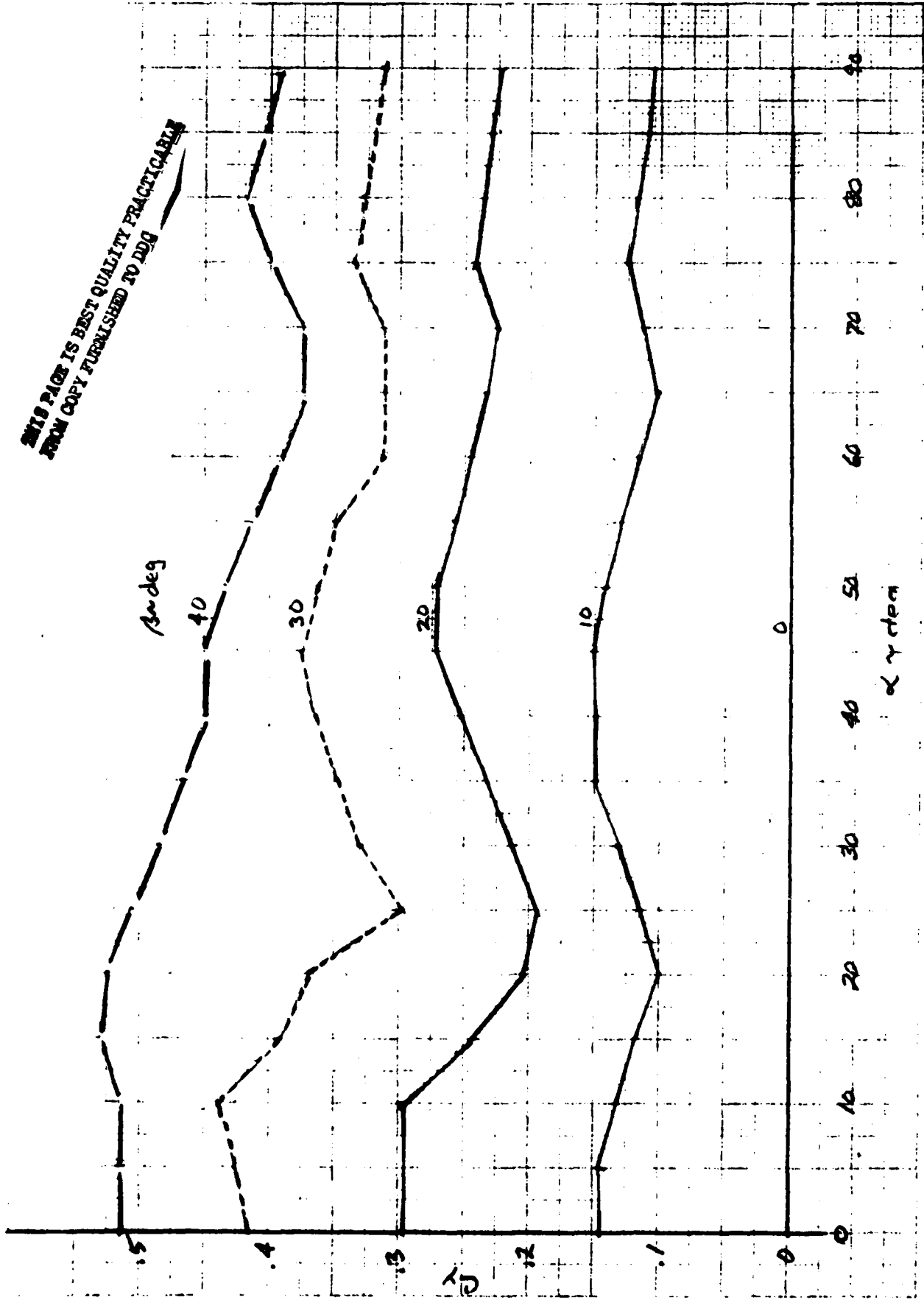


Figure A13.-Pitching moment coefficient as a function of angle of attack and sideslip angle. $i_s = -30$ deg.



THIS PAGE IS BEST QUALITY PRACTICABLE
FROM COPY FURNISHED TO DDD

Angle deg

α deg

Figure A14.- Side force coefficient as a function of angle of attack and sideslip angle. $i_s = 0$ deg.

THIS PAGE IS BEST QUALITY PHOTOGRAPH
FROM COPY FURNISHED TO DOD

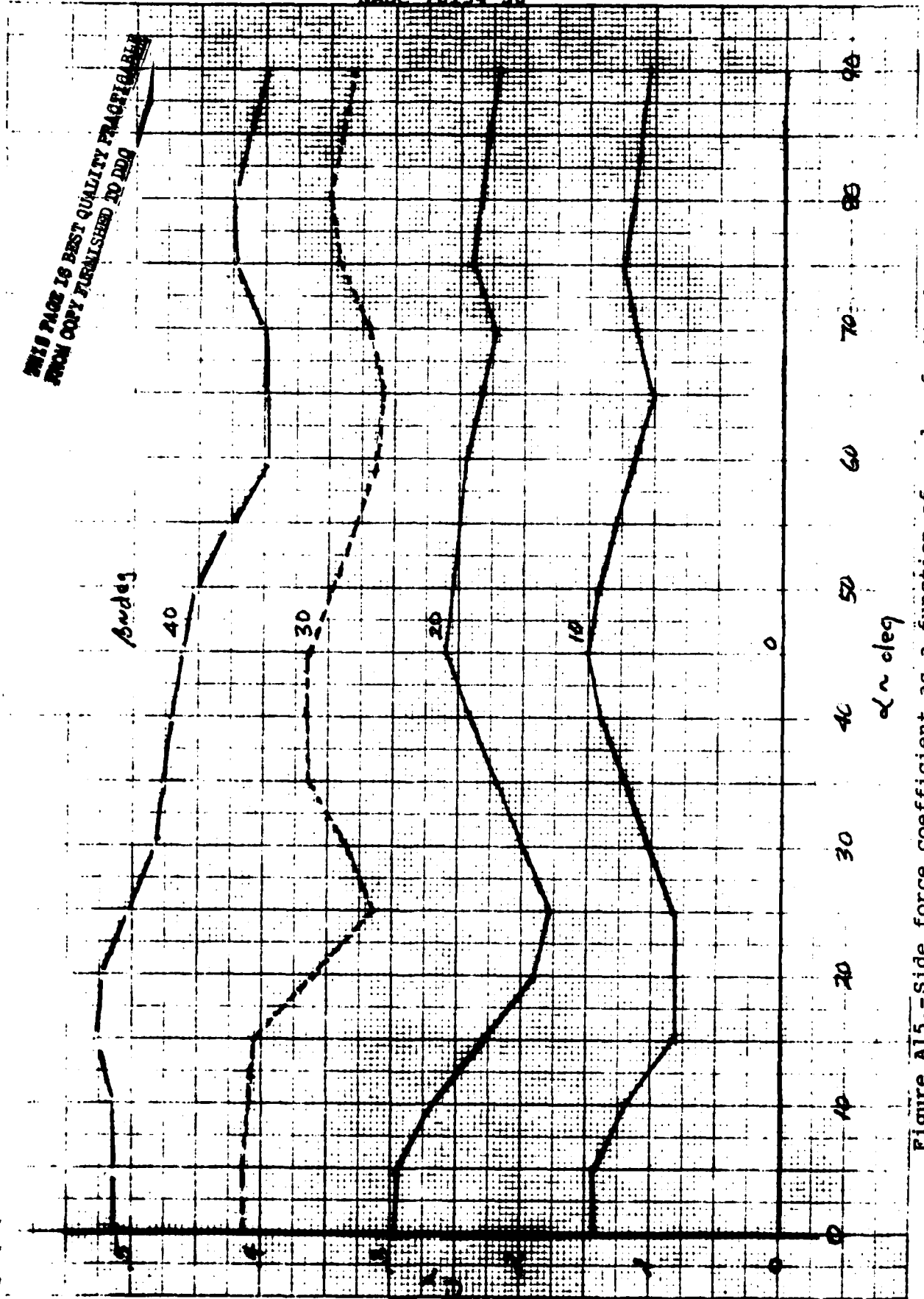


Figure A15.-Side force coefficient as a function of angle of attack and sideslip angle. $i_s = -30$ deg.

THIS PAGE IS BEST QUALITY PRACTICABLE
FROM COPY FURNISHED TO DDG

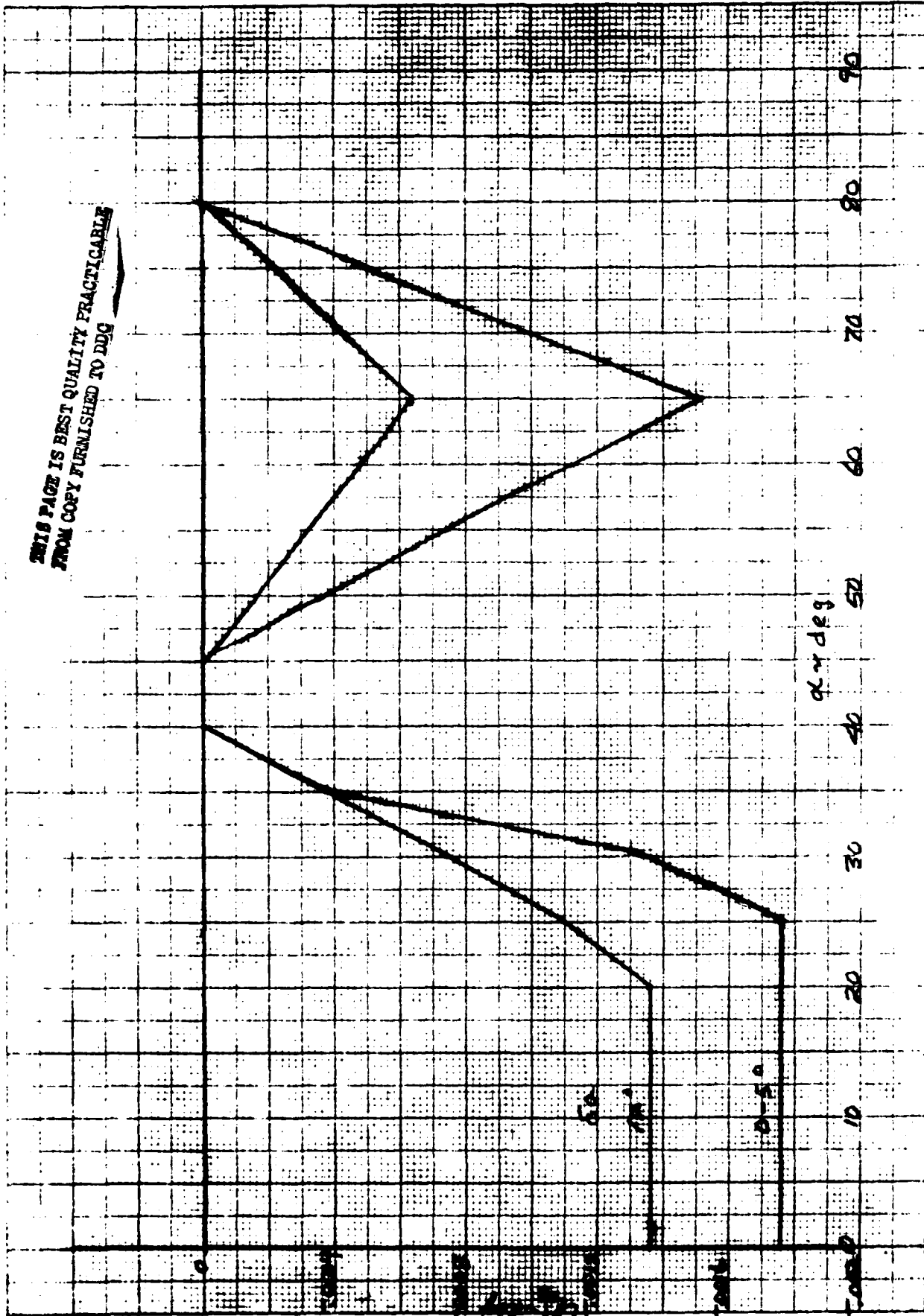


Figure A16.- Rolling moment due to lateral control derivative as a function of angle of attack and control deflection. $i_s = 0$ deg.

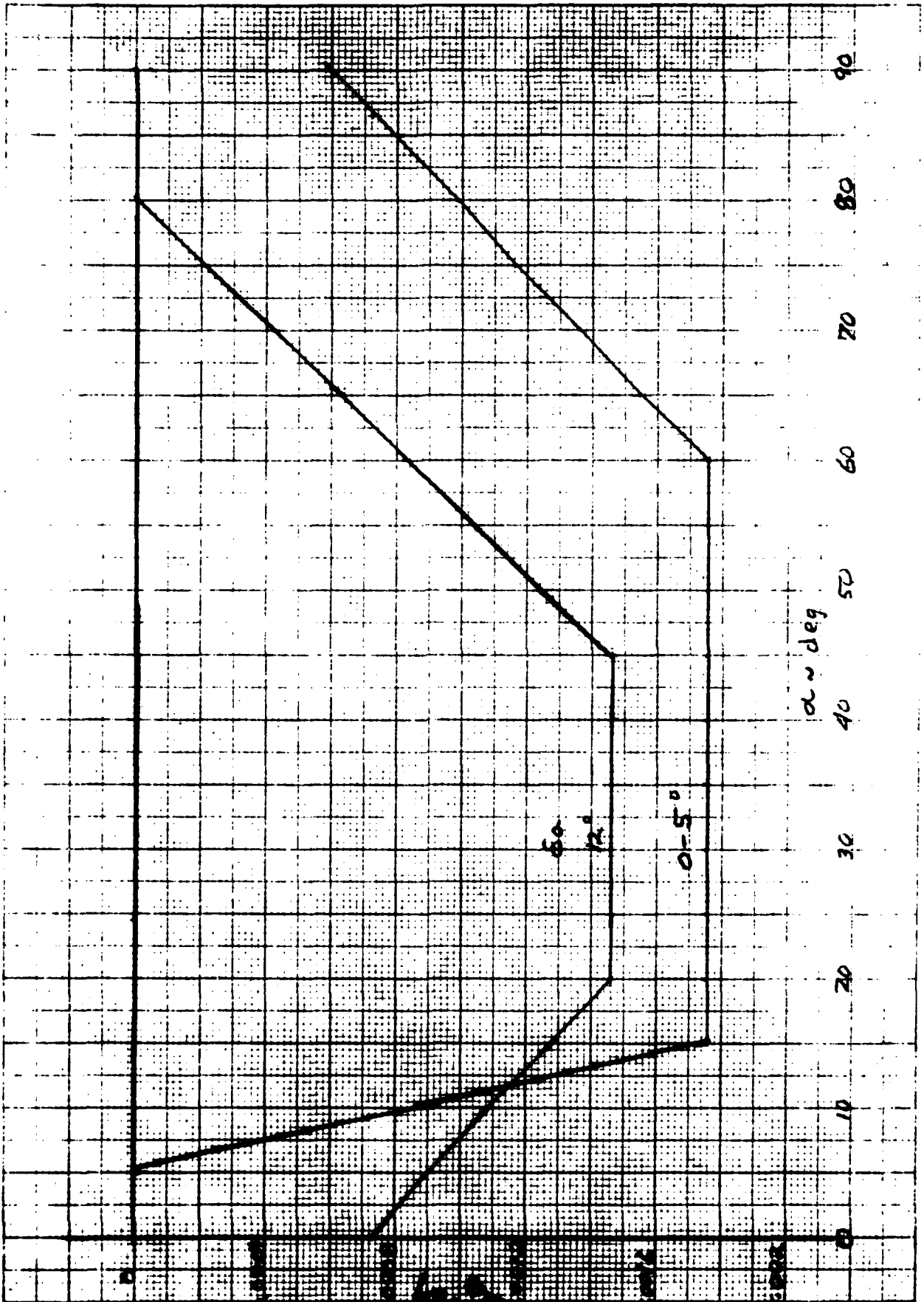


Figure A17.- Rolling moment due to lateral control derivative as a function of angle of attack and control deflection. $i_s = -30$ deg.

THIS PAGE IS BEST QUALITY PRACTICE
FROM COPY FURNISHED TO HQ

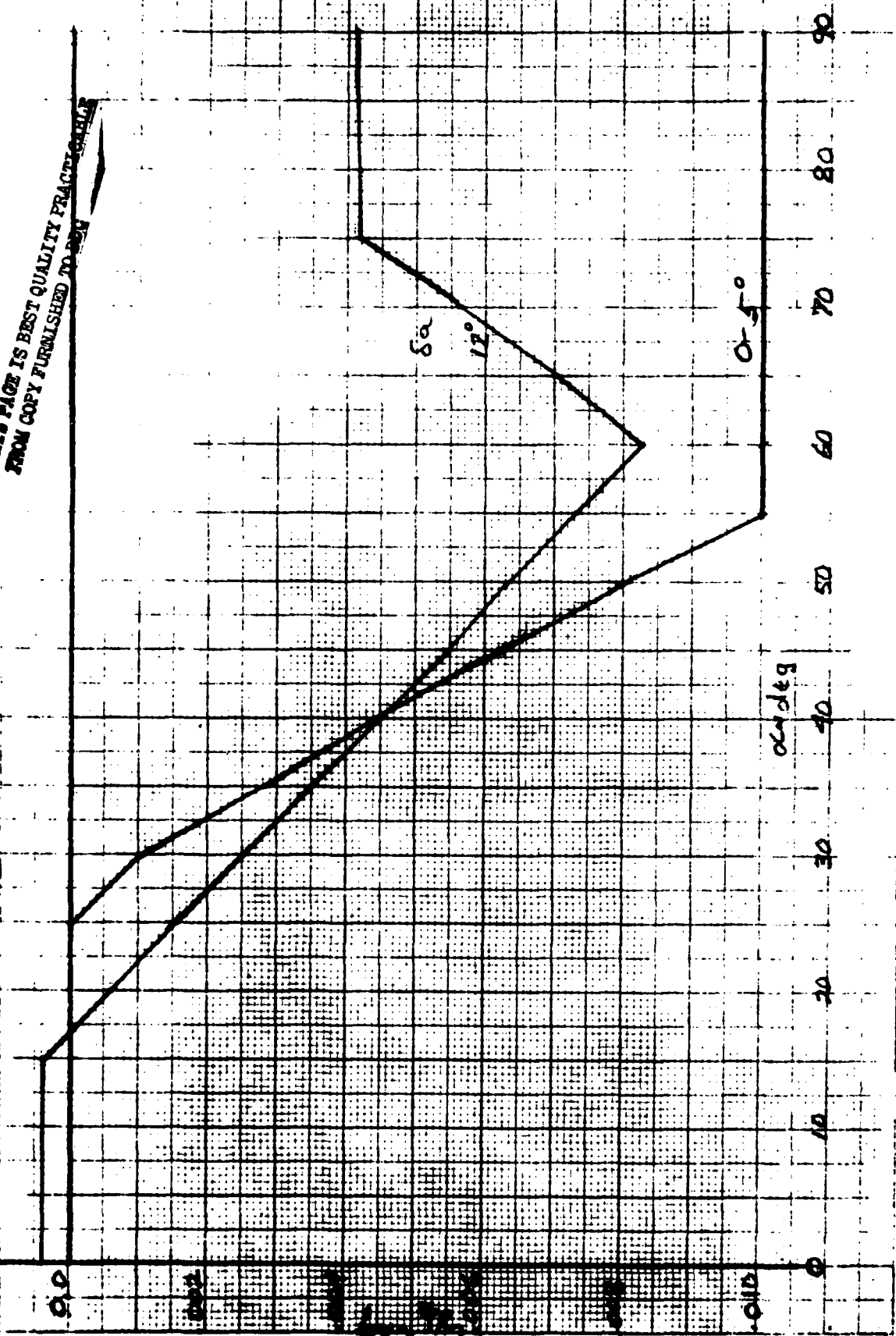


Figure A18.- Side force due to lateral control derivative as a function of angle of attack and control deflection. $i_s = 0$ deg.

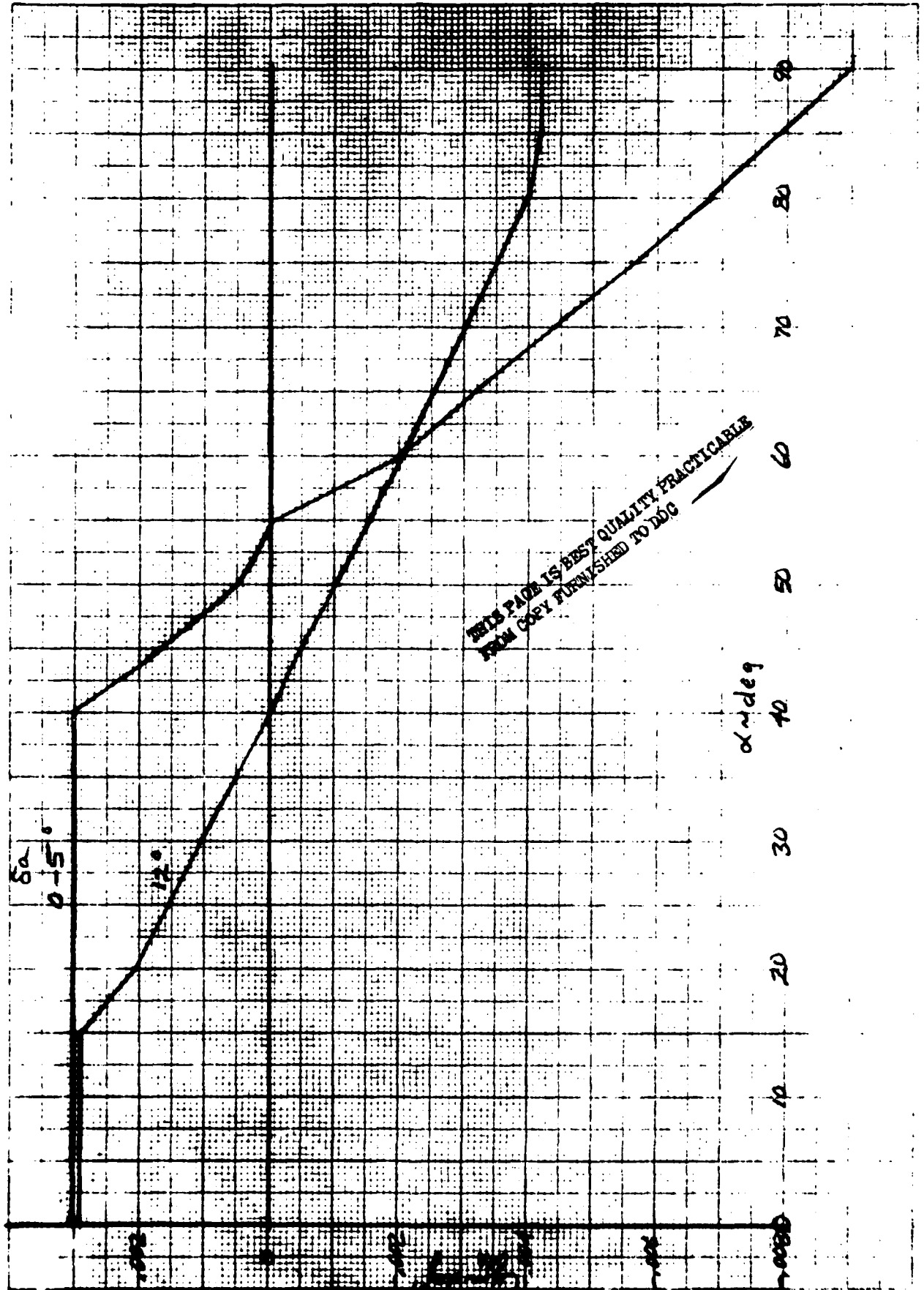


Figure A19.- Side force due to lateral control derivative as a function of angle of attack and control deflection. $i_s = -30$ deg.

THIS PAGE IS BEST QUALITY PRACTICABLE
FROM COPY FURNISHED TO PDG

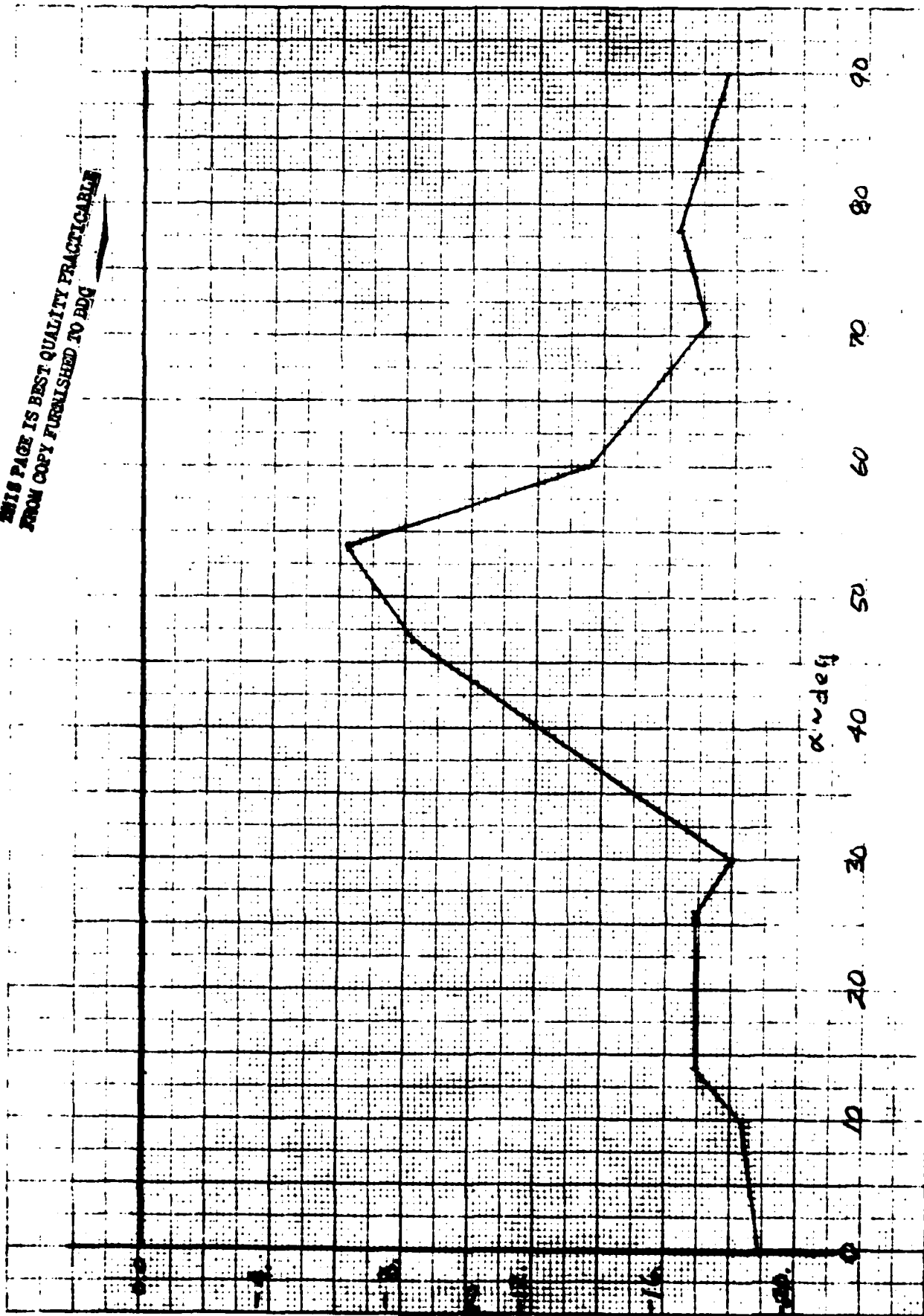


Figure A20:- Damping derivative, C_{mq} , as a function of angle of attack.

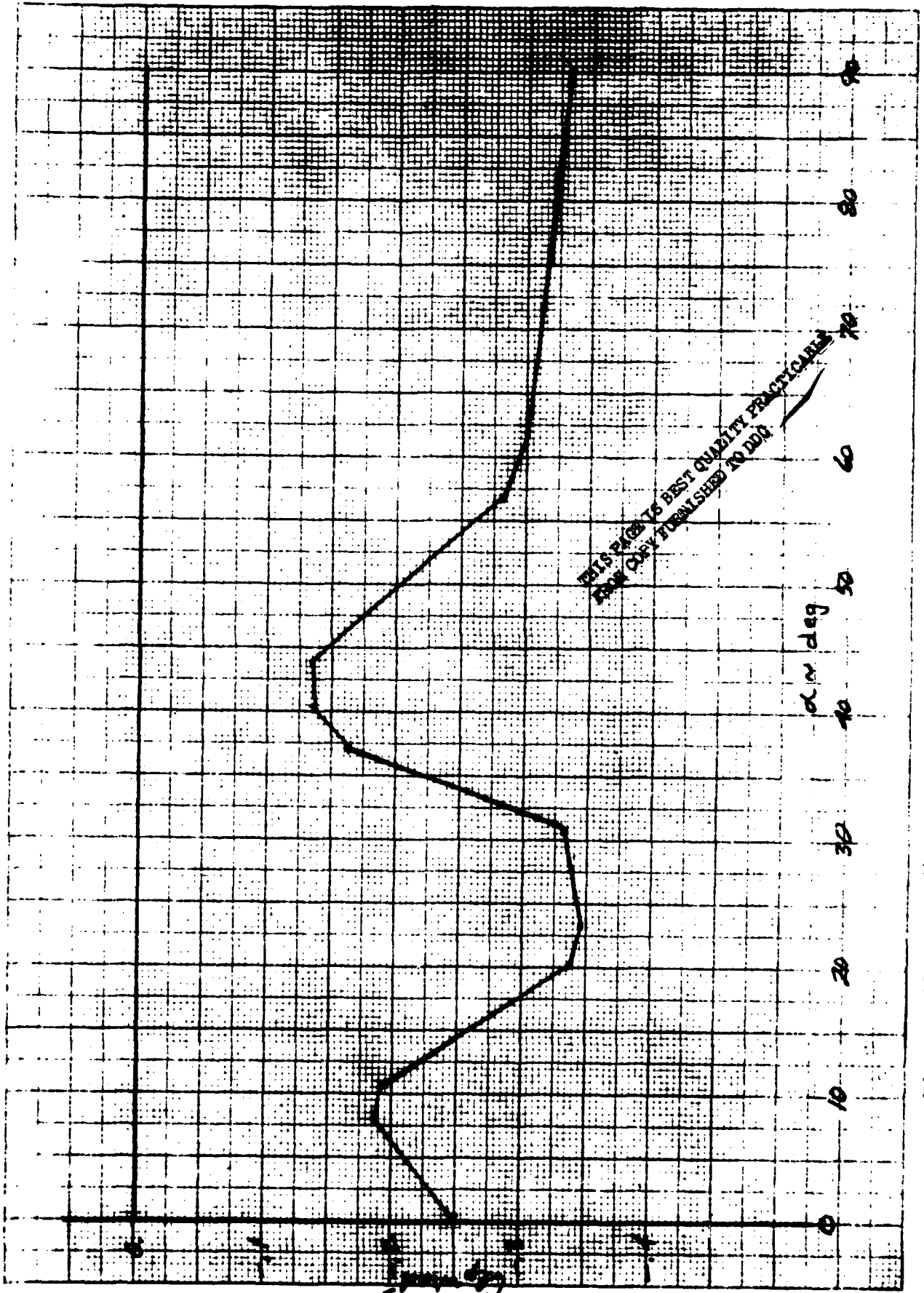


Figure A21.- Damping derivative, $C_{l,p}$, as a function of angle of attack.

THIS PAGE IS BEST QUALITY PRACTICABLE
FROM COPY FURNISHED TO DDG

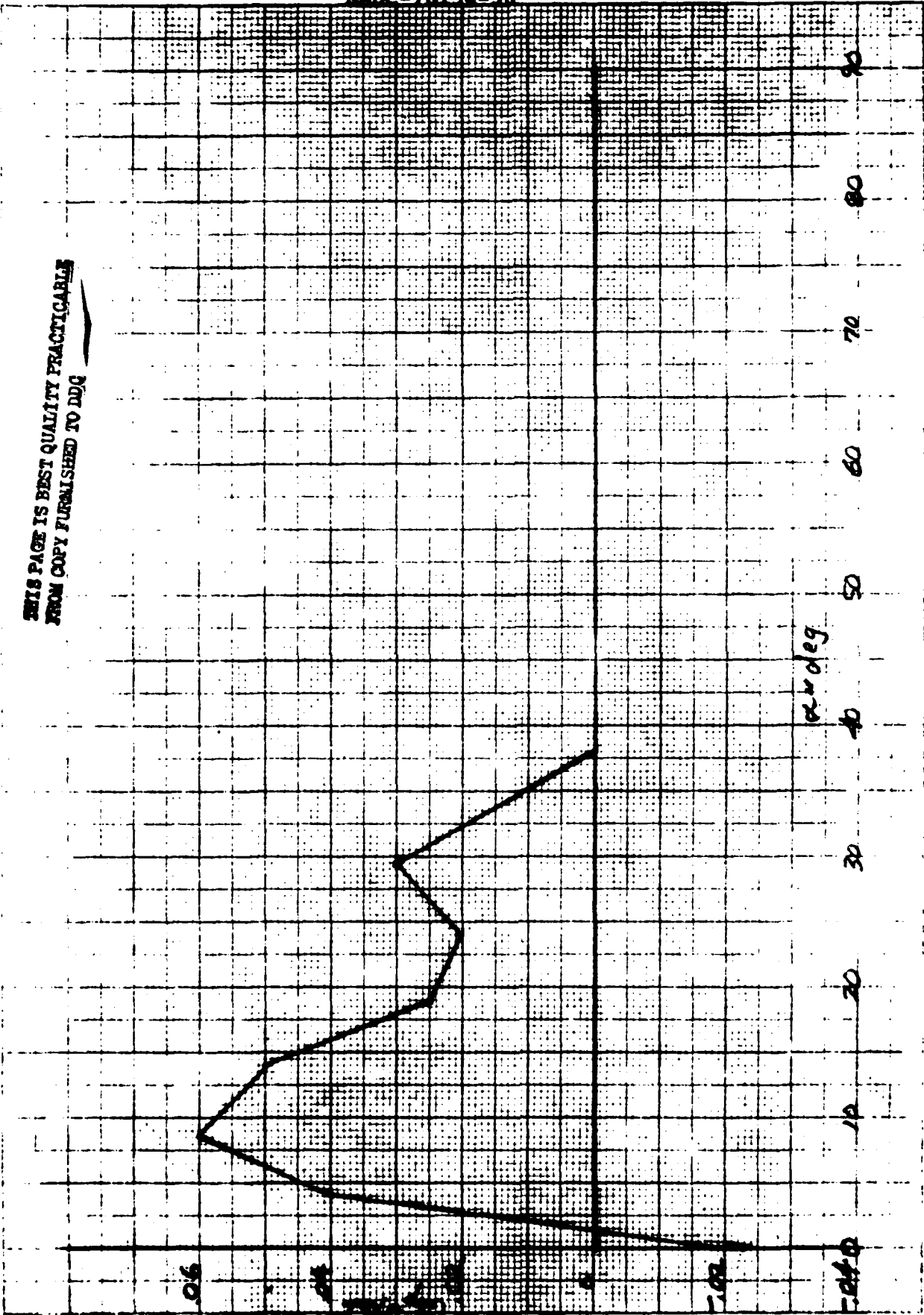


Figure A22.- Cross derivative, C_{np} , as a function of angle of attack.

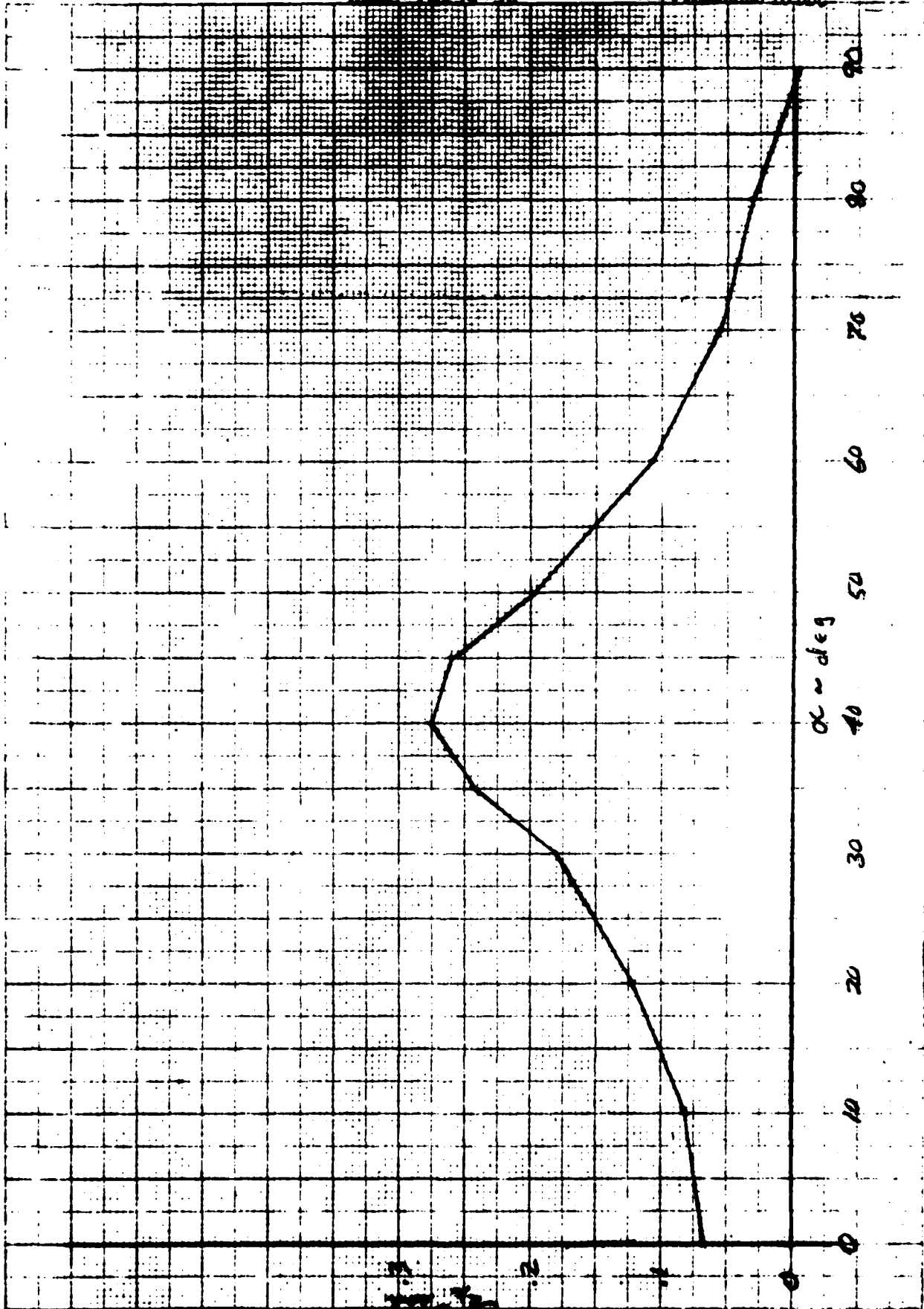


Figure A23.- Cross derivative, C_{l_r} , as a function of angle of attack.

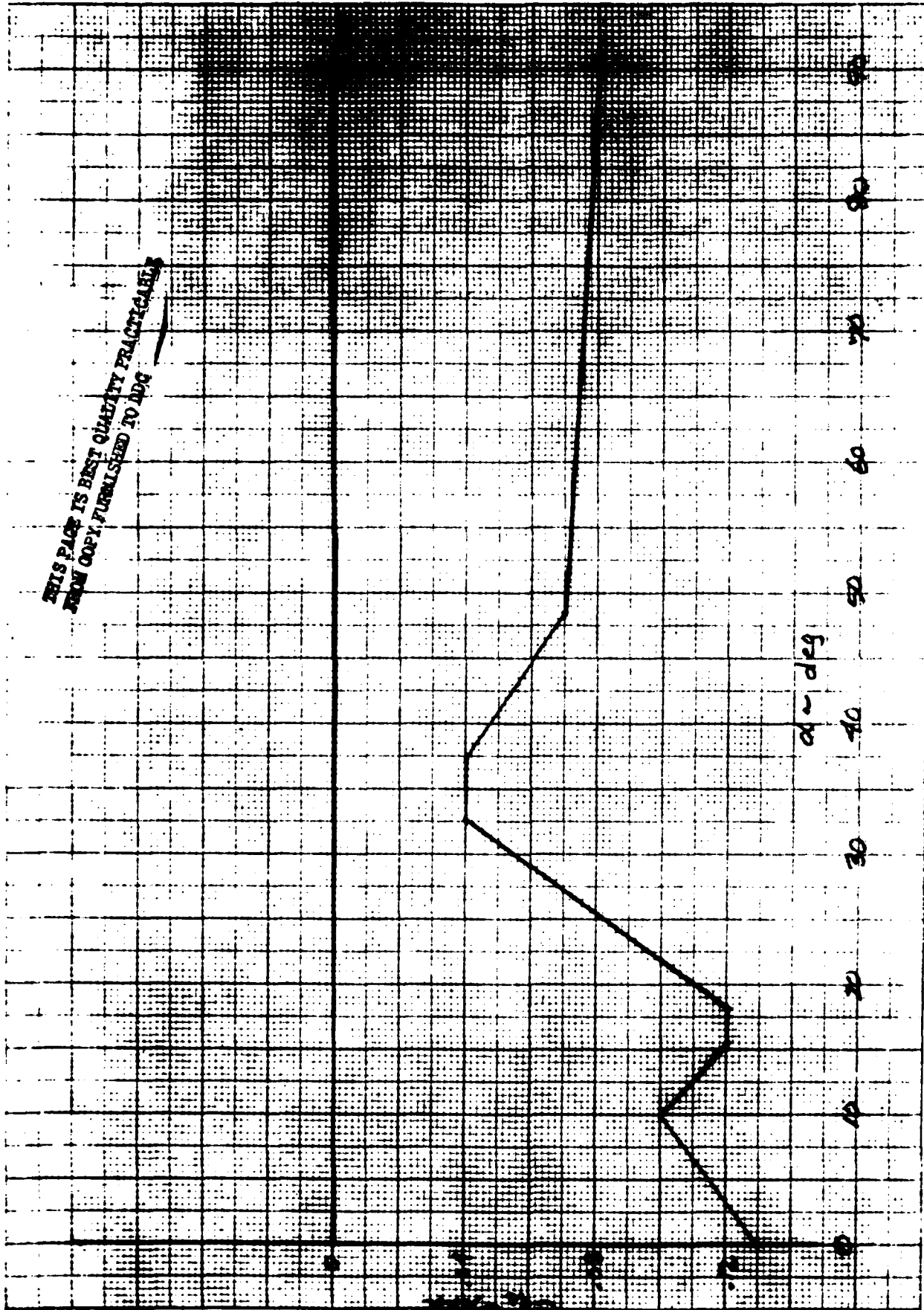


Figure A24.- Damping derivative, $C_{n\dot{\alpha}}$, as a function of angle of attack.